Bayesian Optimization with Early Trial Termination for Speeding Up Parallel Neural Network Training

Anonymous Author(s)
Affiliation
Address
email

Abstract

Training of large neural networks (NNs) is often done in parallel on multiple GPUs. While existing parallel training frameworks easily allow NN training using multi-dimensional parallelism, the challenge remains in finding the optimal hyperparameters, such as the best balance between the sizes of various parallelism dimensions, which would result in the highest training throughput. Due to the large number of possible parallelism configurations (PCs) for a given training scenario, an exhaustive search over them is prohibitively costly. Existing PC optimization methods either require running training trials on a large number of PCs, each of which is costly, or rely on an approximate cost model which may be inaccurate and hardware-specific. To overcome these issues, this paper presents OPPA that can boost the efficiency of Bayesian optimization for optimizing the PC by novelly exploiting (a) the domain knowledge of parallel NN training via parallelism-informed prior beliefs that are general in catering to a variety of NN training scenarios, and (b) early termination of trials involving suboptimal PCs. Despite incorporating these nontrivial efficiency tricks, OPPA is still theoretically guaranteed to achieve sublinear regret. We empirically show that OPPA finds optimal PCs more efficiently than existing methods for parallel training of NNs with varying architectures, training frameworks, and multi-GPU hardware setups.

1 Introduction

Modern advances in deep learning have arisen from the ability to scale neural networks (NNs) to larger sizes. In natural language processing, for example, transformer models [5, 35], large language models (LLMs) [23, 34], and multimodal LLMs [20, 24], which comprise millions to billions of parameters, have shown tremendous success in tasks such as text classification, text generation, and language understanding. These large NNs often cannot be trained on standard machines with a single processor. To scale up, it is necessary to distribute the NN training workload across a cluster of machines and parallelize the training process. Different parallelism techniques for NN training have been proposed, such as that of data [26, 43], pipeline [10, 22], tensor [31], and their combinations which are also referred to as *multi-dimensional parallelism* [17, 28, 31].

To fully utilize the given hardware for reducing the time of NN training, one can maximize its *throughput*, i.e., average number of training steps being run per unit time. The training throughput depends on the selected *parallelism configuration* (PC), which, in large-scale parallel training frameworks [13, 17, 28, 31], is specified by several hyperparameters such as the sizes of various parallelism dimensions. In practice, it is **challenging to accurately determine how the choice of PC affects the training throughput** since such a complex relationship depends on the NN architecture, training data, compute and communications hardware, and the exact implementation of the parallel training framework. *Existing works* that approximate (and optimize) the training throughput of a PC

Submitted to 40th Conference on Neural Information Processing Systems (NeurIPS 2026). Do not distribute.

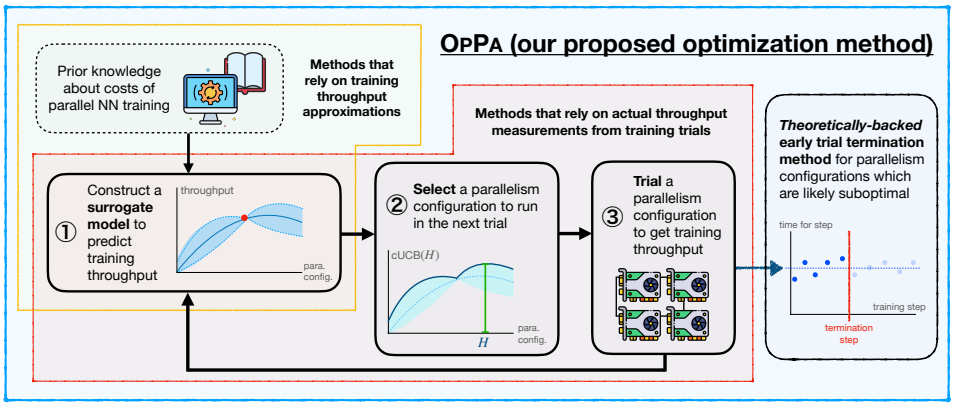

Figure 1: The key idea of OPPA is to exploit domain knowledge of parallel NN training & early trial termination to rapidly find the parallelism configuration (PC) with the highest training throughput.

[15, 41, 44] *require strong assumptions* on the hardware and parallel training implementation, and may not capture all the complex intricacies of parallel training. So, it may not be reliable to rely on any of these works alone to recover the actual optimal PC directly.

In practice, **the most reliable method to consider all possible factors and their interactions during parallel training is to run real training trials** with each PC on the real hardware. Unfortunately, due to the large number of possible PCs, an exhaustive search over them is prohibitively costly. To circumvent this, existing parallel training frameworks have selected a subset of candidate PCs to trial using simplistic optimization algorithms, but *cannot utilize measured throughputs nor prior domain knowledge*, hence inefficiently needing excessive trials to find the optimal PC (Sec. 2).

To efficiently search for the PC with the highest throughput, it is desirable to be able to adaptively select potentially good PCs for trialing and filter out poor candidates using information from trialed PCs. Given these considerations, black-box optimization methods such as Bayesian optimization (BO) (Sec. 2) would be well-suited for the task. However, *a naive use of vanilla BO is still inefficient* as it does not exploit the inherent characteristics of PC trialing nor that of the parallel training process.

This paper presents the OPTIMIZER FOR PARALLELISM CONFIGURATIONS (OPPA) that can adaptively and rapidly optimize the PC for efficient parallel NN training. OPPA (Fig. 1) boosts the efficiency of BO by novelly exploiting *early termination of trials involving suboptimal PCs* and *parallelism-informed prior beliefs* that are general in catering to a variety of NN training scenarios. Despite incorporating these nontrivial efficiency tricks, OPPA is still theoretically guaranteed to achieve sublinear regret. In Sec. 3, we first formulate the problem of finding the optimal PC as one of black-box optimization with black-box constraints. Then, we develop surrogate models representing *parallelism-informed prior beliefs* (based on domain knowledge of parallel NN training) that are general in catering to a variety of hardware setups and training frameworks (Sec. 4.1) and used by BO to select promising PCs for trialing (Sec. 4.2). We also describe the process of trialing a PC and *propose a novel technique to early terminate trials involving suboptimal PCs* with both theoretical and empirical justifications (Sec. 4.3). In Sec. 5, we empirically show that OPPA can be easily used on top of existing parallel training frameworks to find a good PC for training NNs more efficiently than existing methods and vanilla BO without modifications.

2 Background and Related Works

Parallel NN training on GPUs. A large NN can be effectively trained by distributing its workload across multiple GPUs. Different parallelism dimensions split the workload differently, which affects the amounts of computation per GPU, memory required in each GPU, and communication between GPUs. The most basic parallelism technique is data parallelism (DP) [16] where a batch of training data is split and distributed to each device to be separately processed by its local NN replica before gathering the gradients from all devices to update the NN weights. While DP is simple, it requires replicating the NN onto each device, thus incurring additional memory. To resolve this, techniques,

such as the Zero Redundancy Optimizer (ZeRO) [26] in the DeepSpeed package or Fully-Sharded Data Parallel (FSDP) [43], have been proposed to perform some sharding of NN weights or gradients to avoid full NN replication. Furthermore, tensor parallelism (TP) [2, 31] and pipeline parallelism (PP) [10, 22] have been proposed to shard the tensors in the NN and the NN execution pipelines onto multiple devices, respectively. The specific implementations of DP, TP, and PP, such as which tensors (e.g., NN weights, gradients) are sharded or how many shards they are partitioned into, are often manually specified by the user to control the overall throughput. App. A discusses DP, TP, and PP more. Besides, other types of parallelism (e.g., sequence [18], expert [27]) have also been developed.

Multi-dimensional parallelism. Several frameworks [17, 28, 31] have also been developed to combine different types of parallelism into the same training process. These frameworks provide simple interfaces for users to specify the desired *parallelism configuration* (PC) that comprises hyperparameters controlling the execution of the parallel training process, a subset of which specifies the sizes of various parallelism dimensions. These frameworks then automatically handle tensor sharding and execute the parallel training pipeline as per the specified PC. These frameworks may also manage training on multi-node or even heterogeneous hardware. While these frameworks allow practitioners to easily execute parallel NN training, *finding the PC with the highest throughput is challenging* since it depends non-trivially on the NN architecture, training data, GPU specifications, communication bandwidth between GPUs, and the exact implementation of the parallel training framework [17, 19, 36]. For example, DP is ineffective for large NNs since excessive NN replications can cause out-of-memory errors. Also, PP is less effective on smaller NNs as the communication costs between pipeline stages may dominate the computation of the fragmented pipeline.

Optimizing PC. The most accurate way to find the optimal PC would be to trial all possible PCs on the actual training hardware and determine which one yields the highest training throughput. However, this is prohibitively costly since there can be a large number of possible PCs and trialing each PC can be computationally costly. To circumvent this, frameworks such as NeMo [13] and DeepSpeed [28] have implemented methods for automatic PC tuning[1] based on running NN training trials for a few training steps on a number of PCs. The PCs trialed are often either selected non-adaptively (e.g., based on random selection) or adaptively based on a simple surrogate function. However, these methods *cannot efficiently use the measured throughputs of trialed PCs* to perform informed optimization, and therefore still require a large number of training trials to obtain a good PC.

Since training trials are costly, we can consider constructing a surrogate model to approximate the computation and communication costs for different PCs [15, 41, 44]. This would allow us to use domain knowledge to filter out suboptimal PCs and run fewer or even no trials at all. These methods, however, have *implicitly assumed that the surrogate model correctly predicts the actual training throughputs*. This is not possible in practice since the surrogate model cannot capture all the complex intricacies of parallel training. Furthermore, a fixed surrogate model cannot be easily extended to include new hyperparameters into the PC, which is important especially with the ever-growing parallel training literature.

Overview of BO. To efficiently search for the PC with the highest throughput, we utilize BO [7, 8]. BO aims to maximize an expensive-to-query black-box function $\mathcal{R}$ (representing the training throughput over the space of all possible PCs) whose derivative is unknown. The black-box function $\mathcal{R}$ is modeled by a Gaussian process (GP) prior belief specified by its prior mean and covariance [29]. Given the measured throughputs of trialed PCs, we can obtain a predictive distribution of the throughputs (of untrialed PCs) in the form of a GP posterior belief specified by its posterior mean and covariance. Then, the BO algorithm selects a PC for trialing that maximizes a given acquisition function (e.g., expected improvement [11], upper confidence bound [33]) based on the GP posterior belief. Such an acquisition function trades off between exploring unique PCs that have not been queried to predict $\mathcal{R}$ better vs. exploiting PCs likely to have high values of $\mathcal{R}$ so as to efficiently find the optimal PC. App. B gives a more technical overview of GP modeling and BO.

BO is used in a wide range of black-box optimization problems, such as experimental design [14, 25] and material design [42]. More relevant to our work here, BO is also commonly used to optimize the NN architecture to achieve the best performance in a given task [32]. Finding the optimal PC, however, differs in two aspects: (a) The hyperparameters in a PC affecting the training throughput have better-defined mechanics (even if not completely known), which can be partially described

[1] https://docs.nvidia.com/nemo-framework/user-guide/latest/usingautoconfigurator.html, https://www.deepspeed.ai/tutorials/autotuning/

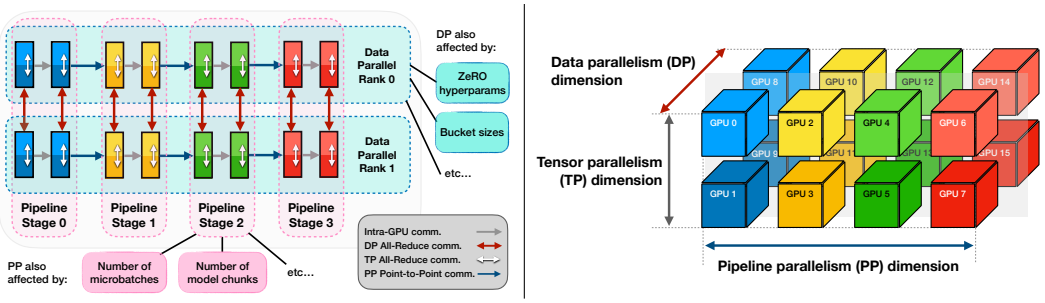

Figure 2: (Left) Visualization of a parallelism configuration (PC) with tunable hyperparameters. (Right) Visualization of GPU allocation for 3D parallelism according to the dimension sizes.

based on domain knowledge. Modeling via a GP allows us to incorporate this knowledge through an informed choice of the GP prior belief, which can reduce the number of trials required. (b) Trialing a PC allows for repeated measurements of the time taken per training step, which are used to calculate the throughput. Running many training steps is costly and may be unnecessary, so an early termination of trials can be adaptively applied to reduce the number of training steps needed to be run. We will elaborate more in the sections to follow.

3 Problem Setting

A parallelism configuration (PC) comprises several tunable hyperparameters found in typical parallel training frameworks and a subset of them determines the *sizes of various parallelism dimensions*, as visualized in Fig. 2. In our work here, we will mainly consider 3D parallelism where `dp`, `tp`, and `pp` denote the sizes of the data, tensor, and pipeline parallelism dimensions, respectively; note that their product $\texttt{dp} \cdot \texttt{tp} \cdot \texttt{pp}$ equals the number `n_gpus` of available GPUs. Also, as demonstrated in our experiments (Sec. 5), other types of parallelism can be included in the PC as well. The remaining hyperparameters determine the *specific implementations of the parallel training framework*, including (but not limited to) hyperparameters in the ZeRO optimizer, the number of model chunks for PP, whether communication overlaps are used, and whether gradient checkpointing is used. App. C.1 lists all of the hyperparameters considered in the PC for our problem, including additional parallelism dimensions that we consider in the experiments.

Let $\mathcal{H}$ be the set of all possible PCs. The goal of our problem is to find the optimal PC $H^* \in \mathcal{H}$ with the *highest training throughput* (i.e., largest average number of training steps being run per unit time) and its *maximum memory usage not exceeding* M_0 (i.e., fitting on the given GPUs). For any PC $H \in \mathcal{H}$, let $\mathcal{R}(H)$ and $\mathcal{M}(H)$ be the throughput and the maximum memory usage, respectively. Then, our problem of finding the optimal PC $H^* \in \mathcal{H}$ can be formulated as one of constrained maximization:

$$\max_{H \in \mathcal{H}} \mathcal{R}(H) \quad \text{subject to} \quad \mathcal{M}(H) \leq M_0 \,.$$

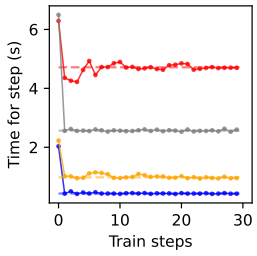

Figure 3: Time taken for each training step for a few training trials with various PCs. Each color represents a different PC used, and the dashed line represents the throughput estimate for that PC. Note the fluctuations in the time taken for each training step.

When querying a PC H, we run a short training trial (instead of training the NN till convergence) to obtain sufficiently accurate estimates of the throughput and maximum memory usage. To estimate the throughput of H, we measure the time taken $t_1, t_2, \ldots, t_{q_{\max}}$ for $q_{\max}$ consecutive training steps and use them to estimate the throughput: $\mathcal{R}(H) \approx \bar{r}_{q_{\max}} \triangleq q_{\max}^{-1} \sum_{j=1}^{q_{\max}} t_j^{-1}$. As shown in Fig. 3, the time taken for each training step fluctuates due to factors like additional overheads during process initialization, fluctuating communication speeds, and unpredictable system behaviors occurring during training. So, it is more reliable to estimate the throughput by averaging the time taken over multiple (rather than a few) training steps. While we can run the full trial with $q_{\max}$ training steps, we can also terminate the trial early after fewer than $q_{\max}$ steps at the cost of a higher variance of the estimator $\bar{r}_q$.

When designing our method, we note two other characteristics of the PC optimization problem:

A Since $\mathcal{R}$ and $\mathcal{M}$ depend on many factors that may be difficult to model or be known exactly, in practice, **their exact forms are only partially known** given the domain knowledge. Therefore, desirable surrogate models for $\mathcal{R}$ and $\mathcal{M}$ **should be able to consider how the actual measurements may deviate from the domain knowledge**. Additionally, the surrogate models should *also be able to quantify its confidence* of any prediction it makes.

B Though a PC can be (and should be) trialed on real hardware, *running a full trial incurs a high cost*. This is especially true with suboptimal PCs since the same number of training steps on a suboptimal PC would incur more time. This motivates us to design an optimization algorithm such that *promising PCs are prioritized for trialing* while **PCs which are likely to be suboptimal are not trialed or are only trialed for a shorter duration**.

4 Method

In this section, we describe OPPA, which exploits parallelism-informed GP prior beliefs and early trial termination to boost the performance of BO in optimizing the PC for parallel training. As summarized in Algorithm 1, OPPA alternates between 3 steps: ① modeling the training throughput and maximum memory usage based on measurements via *parallelism-informed GP prior beliefs*, ② selecting the next PC to trial via BO, and ③ running an NN training trial (and *early terminating it if suboptimal*) to obtain measurements for the throughput and maximum memory usage for the selected PC.

Algorithm 1 OPPA (shortened version of Algorithm 4)

Generate $\mathcal{H}$ of all valid PCs
for $i = 1, 2, \ldots$ **do**
  // Step ① – Modeling $\mathcal{R}$ and $\mathcal{M}$ (Sec. 4.1)
  Obtain GP predictive/posterior beliefs of $\mathcal{R}$ and $\mathcal{M}$ (22) from *parallelism-informed GP prior beliefs* using measurements of trialed PCs
  // Step ② – Selecting the next PC to trial (Sec. 4.2)
  Select $H_i \in \mathcal{H}$ with cUCB criterion (27)
  // Step ③ – Trialing the selected PC (Sec. 4.3)
  for training steps $q = 1, \ldots, q_{\max}$ **do**
    Measure training step time $t_{i,q}$
    if $I_{i,q} = 0$ **then terminate trial** // From (3)
  if budget exhausted **then break**
return H_i with the best measured throughput

4.1 Constructing Surrogate Models

In Step ①, we construct surrogate models to predict the throughput and the maximum memory usage. As suggested in A, to explicitly capture the deviations from the domain knowledge, we decompose the actual throughput $\mathcal{R}$ and maximum memory usage $\mathcal{M}$ into

$$\mathcal{R}(H) = \widehat{\mathcal{R}}(H; \theta_{\mathcal{R}}) + f_{\mathcal{R}}(H) \qquad \text{and} \qquad \mathcal{M}(H) = \widehat{\mathcal{M}}(H; \theta_{\mathcal{M}}) + f_{\mathcal{M}}(H) \tag{1}$$

where the functions $\widehat{\mathcal{R}}$ and $\widehat{\mathcal{M}}$ (with hyperparameters $\theta_{\mathcal{R}}$ and $\theta_{\mathcal{M}}$) capture the domain knowledge of parallel NN training, and $f_{\mathcal{R}}$ and $f_{\mathcal{M}}$ capture the unknown deviations from the domain knowledge.

Domain knowledge. The functions $\widehat{\mathcal{R}}$ and $\widehat{\mathcal{M}}$ aim to, respectively, *predict* $\mathcal{R}$ and $\mathcal{M}$ using only the domain knowledge of parallel NN training. Hence, *they are not expected to give completely accurate predictions but instead capture general trends in any given NN training scenario*; any factors not accounted for would be captured in the unknown deviation terms anyway, to be described below. In practice, OPPA allows the predictions of $\widehat{\mathcal{R}}$ and $\widehat{\mathcal{M}}$ to be improved by incorporating additional domain knowledge from practitioners with more expertise in parallel NN training. Consequently, this would enable OPPA to more rapidly find the optimal PC.

For OPPA, we provide default choices of $\widehat{\mathcal{R}}$ and $\widehat{\mathcal{M}}$ by considering parallel NN training under idealized conditions: For $\widehat{\mathcal{R}}$, we consider the time taken per training step for the computation $\widehat{\mathcal{T}}_{\text{comp}}$ and for the communication $\widehat{\mathcal{T}}_{\text{comm}}$, which can be combined to approximate the throughput as $\widehat{\mathcal{R}}(H; \theta_{\mathcal{R}}) = \left[\widehat{\mathcal{T}}_{\text{comp}}(H; t_{\text{c}}) + \widehat{\mathcal{T}}_{\text{comm}}(H; \mathbf{C})\right]^{-1}$ where $\theta_{\mathcal{R}} = \{t_{\text{comp}}, \mathbf{C}\}$ are learned hyperparameters. For $\widehat{\mathcal{T}}_{\text{comp}}$, we consider the additional computation time arising from the pipeline bubble in PP [22]. For $\widehat{\mathcal{T}}_{\text{comm}}$, inspired by [38], we consider an idealized training scenario visualized in Fig. 2, which assumes the NN to contain roughly identical blocks, and considers the communication from the All-Reduce operations involved in DP and TP, and point-to-point communications involved in PP. We separately model the intra- and inter-node connections, collapsing the constants for specific communication types into $\mathbf{C}$; further details are in App. D.1. For $\widehat{\mathcal{M}}$, we consider the memory required per GPU to store the NN parameters and gradient values for backpropagation, as detailed in App. D.2.

The reason for our choices of $\widehat{\mathcal{R}}$ and $\widehat{\mathcal{M}}$ is that they are general in catering to NN training scenarios with varying model, hardware, and network configurations, while exhibiting a simple analytical form whose forward pass is cheap. We also *use learnable parameters* (as opposed to fixed constants) to capture approximate cost multipliers which depend on the model and training data sizes, and intra- and inter-node network communications, each of which vary across different training scenarios. The design choice allows the prior beliefs to capture the general trends of the throughput and maximum memory usage well enough especially when combined with the learned unknown deviation, while not incurring too much additional computational costs during the PC optimization process.

Unknown deviations from domain knowledge. Due to incomplete domain knowledge to fully describe a parallel training process, we learn the deviations $f_{\mathcal{R}}$ and $f_{\mathcal{M}}$ of the actual measurements from the domain knowledge using real training trials by modeling them as Gaussian processes (GPs). The benefit of using a GP is twofold. First, a GP is typically flexible enough to model unknown functions that may not have an analytical form. Second, a GP can quantify its uncertainty, which allows the surrogate model to determine how much it knows about the throughput of a certain PC. This allows OPPA to potentially trial PCs whose throughput it is more uncertain about.

To model $f_{\mathcal{R}}$ and $f_{\mathcal{M}}$, we use a GP with zero mean such that the resulting GPs will be "centered" around the prior means. For their prior covariances, we concatenate each hyperparameter value in H, then scale each dimension to be between 0 and 1 to form an embedding $e(H)$. Given the embedding, we then use the Matern kernel [29] with $\nu = 5/2$ where the distance between two PCs is the Euclidean distance of their corresponding embeddings with kernel hyperparameters θ_k. In App. D.3, we provide the equation for the Matern kernel, and describe the informativeness of the distance between embeddings in distinguishing between PCs as reflected by the empirical results.

The additive decomposition of the domain knowledge and the unknown deviation in (1) implies that $\mathcal{R}$ and $\mathcal{M}$ are samples from **parallelism-informed prior beliefs**, given by the GPs

$$\mathcal{R} \sim \mathcal{GP}\big(\widehat{\mathcal{R}}(\cdot\,;\,\theta_{\mathcal{R}}), k(\cdot,\cdot\,;\,\theta_k)\big) \qquad \text{and} \qquad \mathcal{M} \sim \mathcal{GP}\big(\widehat{\mathcal{M}}(\cdot\,;\,\theta_{\mathcal{M}}), k(\cdot,\cdot\,;\,\theta_k)\big). \tag{2}$$

Using measurements of trialed PCs, we find the optimal hyperparameters $\{\theta_{\mathcal{R}}, \theta_{\mathcal{M}}, \theta_k\}$ by maximizing the marginal log-likelihood [29] and the subsequent GP posterior beliefs for the throughput and the memory usage for any PC $H \in \mathcal{H}$, which would be normal distributions with their respective mean and variance functions, as stated in App. D.4.

4.2 Selecting the Next PC to Trial

In Step ②, the next PC to trial is chosen based on the surrogate models constructed in ① using BO. The next PC $H_i \in \mathcal{H}$ to trial in round i is chosen to be the PC which maximizes the constrained upper confidence bound (cUCB) [33, 37], which we detail further in App. E.1. The cUCB criterion considers a balance between *exploration* of PCs which have not been trialed, and *exploitation* of PCs which are similar to those with already high throughputs [8, 11]. With this balance, OPPA is able to trial enough PCs to construct reasonable surrogate models for $\mathcal{R}$ and $\mathcal{M}$, while still being able to trial enough promising PC candidates to find one with the maximum training throughput. This allows the optimization to be more guided and more efficient, satisfying the requirement in B.

4.3 Trialing the Next PC, while Terminating Suboptimal Trials Earlier

Finally, in Step ③, we run a training trial on the PC H_i chosen in Step ② for q_{max} training steps, and measure the time taken for each training step as $t_{i,1}, \ldots, t_{i,q_{\text{max}}}$. We then use these measurements to obtain an estimate of the throughput $\bar{r}_{i,q_{\text{max}}}$ where $\bar{r}_{i,q} = q^{-1} \sum_{j=1}^{q} t_{i,j}^{-1}$ and whose variance $\sigma^2_{\bar{r}_{i,q}}$ we detail in App. F.1. In practice, as demonstrated earlier in Fig. 3, the actual measured time for a sequence of training steps may contain outliers which can skew the throughput estimates. As we discuss in App. F.2, to make our estimate more accurate, we remove outlier values of $t_{i,j}$ before computing the throughput estimate. Meanwhile, the maximum memory usage m_i across all training steps is retrieved by calling `torch.cuda.max_memory_allocated()`.

Early trial termination. In practice, some PCs do not need to be trialed for the full q_{max} steps since fewer training steps are sufficient to determine that the PC is suboptimal. This is because $\bar{r}_{i,q}$ is an estimator for the throughput $\mathcal{R}(H_i)$ whose variance $\sigma^2_{\bar{r}_{i,q}}$ decreases as q gets larger. Intuitively, this means that after a certain number of steps, $\bar{r}_{i,q}$ will estimate $\mathcal{R}(H_i)$ with low enough variance that we can determine that it would not improve upon the best PC found so far.

To save time on these trials, we consider early trial termination where the training trial only continues if the estimated throughput is above some threshold. Formally, define an indicator variable

$$I_{i,q} = \mathbb{1}\left[(q \leq q_{\text{min}}) \vee \left(\bar{r}_{i,q} \geq \max_{l \in \{1,\ldots,i-1\}} \bar{r}_{l,\hat{q}_l} + \tau_q\right)\right]. \tag{3}$$

In words, $I_{i,q} = 1$ when fewer than q_{min} training steps have been ran, or when the estimated throughput of H_i is likely to be higher than the throughputs found so far. We can continue the qth training step as long as $I_{i,q-1} = 1$, and terminate the training trial at the step $\hat{q}_i$ when $I_{i,\hat{q}_i} = 0$, which is when H_i is unlikely to improve the best PC found so far. As we intuitively describe in App. F.3.1, this also corresponds to when more training steps are unlikely to provide additional information about the optimal PC or optimal throughput. This saves computation time in practice while still allowing the BO algorithm to recover the optimal PC, as formalized below:

Theorem 4.1 (Informally stated in terms of $\mathcal{R}$)**.** *Consider a simplified case where $\mathcal{M}(H) \leq M_0$ for all $H \in \mathcal{H}$. Let N be the number of PCs trialed so far. Then, there exists some choice of $\{\tau_q\}_{q=1}^{q_{\text{max}}}$ such that, with high probability, the cumulative regret is $\sum_{i=1}^{N} (\mathcal{R}(H^*) - \mathcal{R}(H_i)) = \widetilde{\mathcal{O}}\left(\sqrt{N/q_{\text{min}}}\right)$, and for all $i = 2, \ldots, N$, if $\mathcal{R}(H_i) < \max_{k \in \{1,\ldots,i-1\}} \mathcal{R}(H_k)$, then $\hat{q}_i < q_{\text{max}}$.*

In App. F.3.2, we prove a more general version of Thm. 4.1 (where $\mathcal{R}$ can instead be any function with a bounded RKHS norm), and provide empirical verification for early termination. Note that while Thm. 4.1 assumes $\mathcal{M}(H) \leq M_0$ for all $H \in \mathcal{H}$, the throughput cannot be measured when $\mathcal{M}(H) > M_0$ anyway (since the run would encounter an out-of-memory error), and so can be omitted in the theoretical analysis for convenience. Thm. 4.1 shows that sublinear regret can be achieved even with early termination, which means that OPPA will be able to recover the PC with the best throughput while allowing efficiency gains in practice. Furthermore, it also shows that PCs whose throughput is smaller than those of PCs already trialed will likely have their trials terminated early, allowing OPPA to save resources from trialing suboptimal PCs as mentioned in B. We present the complete pseudocode for OPPA incorporating steps ①, ②, and ③ in App. G.

5 Experiments and Discussion

In this section, we present the results for OPPA when used to find the optimal PC for training NNs on multi-GPU systems. We consider optimizing the PC for training NNs with different architectures and sizes, on various hardware configurations with varying number of GPUs, and on different parallel training frameworks. Detailed setups for the training scenarios are found in App. H.1.

We compare OPPA against RANDOM (random selection), XGBOOST (adaptive selection based on XGBOOST surrogate model [3] as used by DEEPSPEED [28]), COST-MODEL (method which solely relies on the cost model of the throughput), and VANILLA-BO (BO without any additional modifications). App. H.2 provides detailed descriptions of these methods.

In each case, we plot the best obtained throughput (in training steps per second) vs. how long the optimization has been run rather than vs. the number of PCs that have been trialed. We do so since how long the optimization has been run is a better reflection of the costs involved in optimizing the PC, as it captures both the time required to run the optimization algorithm and the time to run the training trials. The latter also includes the time to initialize the NN training, to run the training steps, and to switch the training to a different PC, and will also be higher if the algorithm trials more PCs or trials suboptimal PCs. Nonetheless, plots for the achieved throughput vs. the number of trials run are in App. I.1. The model loss are independent of the chosen PC and thus are not reported.

Training on single-node setups. We first consider NN training on a single node. Fig. 4a shows the results for finding the optimal PC for training the BERT model [5]. We see that OPPA, which exploits a parallelism-informed prior and early termination mechanism, is able to outperform the non-adaptive and adaptive methods, and even outperforms vanilla BO. We find that OPPA automatically prioritizes PCs with only DP which matches our intuition that DP should be adequate for smaller NNs. Fig. 4b considers the Qwen model [39] where OPPA again finds a better PC compared to the other methods. Due to a larger model, OPPA now prefers a mix of DP and PP to reduce memory use while incurring minimal additional inter-GPU communications. We present the PCs selected by OPPA in App. I.2.

To visualize the efficiency gains of OPPA, in Fig. 5a, we see that OPPA is able to trial many more PCs in a given time period when compared to other methods due to the early termination of suboptimal trials to avoid wasting time. While OPPA will perform more switching between PCs to trial, the cost

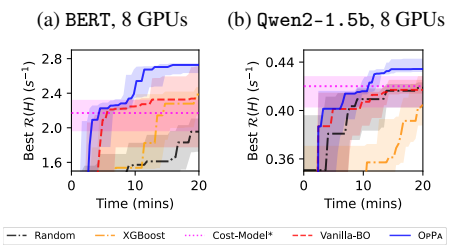

Figure 4: The best obtained throughput (higher is better) vs. the duration each method has been run for, when training on a system with a single node on COLOSSAL-AI [17]. For each method, the line shows the median of repeated trials, while the error band shows the quartiles.

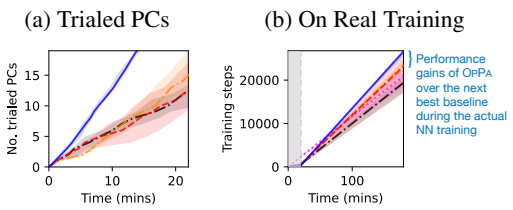

Figure 5: Efficiency of OPPA. The plots show statistics for the experiments in Fig. 4a. Fig. 5a shows the no. of PCs trialed by each method during its run. Fig. 5b shows the no. of training steps that can be run by each method during optimization (the shaded gray region on the left) and during subsequent NN training using the optimized PC (unshaded region on the right). The legend is the same as in Fig. 4.

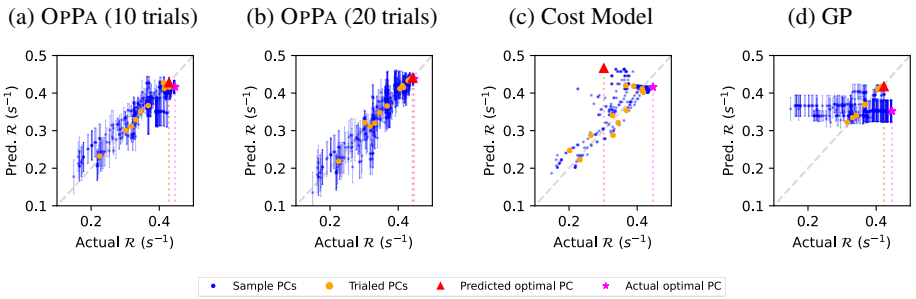

Figure 6: Predicted throughputs from different surrogate models vs. the measured throughputs for the `Qwen2-1.5b` example (Fig. 4b). Figs. 6a and 6b show the predictions from OPPA after 10 and 20 trials respectively, with error bars for the predictive variance. Fig. 6c shows the predictions from the cost model alone, while Fig. 6d shows the predictions from using a GP alone (both after 20 trials).

incurred by this switching is less than the time saved by not running all training trials in full, allowing OPPA to trial more PCs overall. Along with the parallelism-informed GP prior beliefs to efficiently filter out suboptimal PCs, OPPA returns a PC with a higher throughput, which in turn allows more training steps to be run in the subsequent training even after just 20 minutes of PC optimization, as shown in Fig. 5b. This demonstrates the necessity of OPPA to achieve faster parallel training.

Flexibility across different parallel training frameworks and NN architectures. In App. I.3, we run similar experiments as that in Fig. 4, except that we perform training on the NEMO framework [13] where we additionally optimize for the size of the sequence parallelism dimension [18] in the PC. Meanwhile, in App. I.4, we compared OPPA with other methods in optimizing the PC for Vision Transformers and Mixture of Experts (MoE). Optimizing PC for MoE training is particularly interesting since the PC now includes the size of expert parallelism dimension [27]. In all of these scenarios, OPPA outperforms the other baselines. This demonstrates that the surrogate models used by OPPA will not overfit to a specific training scenario, but instead can cater to a wide variety of training frameworks, various NN architectures, and even unseen hyperparameters in a PC.

Accuracy of surrogate models. Figs. 6a and 6b compare the throughput predicted by OPPA with the actual measured throughput. We see that even after 10 trials, the predictions made by our surrogate models already correlate well with the measured throughput. As we progress, the prediction becomes more accurate, especially among PCs with high throughput where more trials are being run, which allows OPPA to better identify the optimal PCs. In contrast, a cost model alone (Fig. 6c) can capture general trends of $\mathcal{R}(H)$ but not all complex intricacies of the throughput, while a GP alone (Fig. 6d) is unable to learn meaningful interpolations for $\mathcal{R}(H)$. The shortcomings of these two surrogate models create a mismatch between the predicted optimal PC and the actual optimal PC. We further discuss the quality of the surrogate models for the throughput and maximum memory usage in App. I.5.

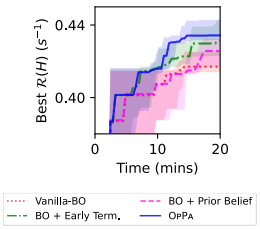

Figure 7: Effects of early termination and parallelism-informed GP prior beliefs on the ability of OPPA to optimize the throughput for `Qwen2-1.5b` training.

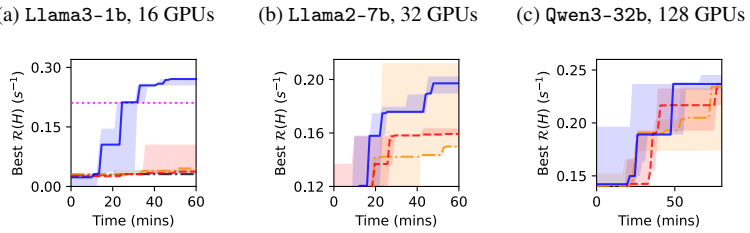

Figure 8: The best obtained throughput vs. the duration each method has been run for, when training NNs on multiple nodes. Figs. 8a and 8b was ran on COLOSSAL-AI [17], while Fig. 8c was ran on NEMO [13] with sizes of sequence and context parallelism dimensions also being tuned. The legend is the same as in Fig. 4. Some methods were not ran for results in Figs. 8b and 8c due to the available computational budget.

Effects of each component in OPPA. In Fig. 7, we performed ablation studies to isolate the effects from each proposed component in OPPA. We see that without early termination, BO would spend more time on suboptimal trials, resulting in a slower search process. Similarly, without the GP prior beliefs, we would be less informed about PCs which may be optimal, requiring more time to find the optimal PC. Additional results are presented in App. I.7. We also show the effects of $q_{\min}$ on the performance of OPPA in App. I.8, demonstrating minimal degradation for small $q_{\min}$.

Training on multi-node setups. In addition to training on single-node setups, we also tested OPPA on optimizing the PC on multi-node setups. In these cases, the additional communication costs makes the throughput computation less straightforward, while larger number of feasible PCs complicates the optimization problem. In Fig. 8a, we show the results for optimizing the PC for training a smaller model [9] with 1 billion parameters on a commodity cluster with 16 GPUs, which is a typical setup found by practitioners with existing hardware in practice. Meanwhile, Figs. 8b and 8c are the results for optimizing the PC to train larger models [34, 40] on high-performance computing clusters with 32 and 128 GPUs, respectively. In all of these cases, OPPA outperforms other baselines, and also does so more consistently (i.e., smaller variance in the resulting throughput), demonstrating its robustness. This trend is observed across different scales of hardware setup, and even across training frameworks or when including new parallelism dimensions in the PC (e.g., the experiment for Fig. 8c which includes six types of parallelism). We also see that vanilla BO outperforms other non-BO methods due to its ability to balance exploration and exploitation, however remaining worse than OPPA.

In Fig. 9, we also demonstrate that OPPA is additionally able to outperform cost model-based methods such as AMP [15] and NNSCALER [19]. This shows the superiority of adaptive methods which can effectively incorporate the measured throughput from actual training trials as opposed to solely using cost models, and the non-trivial components exploited by OPPA that allow for this boost in performance.

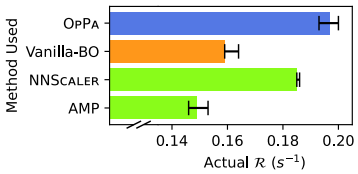

Figure 9: Obtained $\mathcal{R}$ from OPPA compared to those from cost model-based methods for `Llama2-7b` training with 32 GPUs. The results reported for BO and OPPA are the same from Fig. 8b.

6 Conclusion

We have presented OPPA, which improves upon constrained Bayesian optimization by exploiting parallelism-informed GP prior beliefs and an early termination mechanism to efficiently optimize the parallelism configuration and achieve the highest training throughput across a variety of NN architectures, training frameworks, and hardware setups. As demonstrated, OPPA can also be easily adapted to optimize other unseen hyperparameters in a PC as well. We believe the parallelism-informed GP prior beliefs can be embedded with more domain knowledge of specific parallel training frameworks or knowledge of specific NN architectures, which would boost the performance of OPPA further.

References

[1] M. Balandat, B. Karrer, D. R. Jiang, S. Daulton, B. Letham, A. G. Wilson, and E. Bakshy. BoTorch: A Framework for Efficient Monte-Carlo Bayesian Optimization. In *Proc. NeurIPS*, 2020.

[2] Z. Bian, Q. Xu, B. Wang, and Y. You. Maximizing Parallelism in Distributed Training for Huge Neural Networks. 2021. arXiv:2105.14450.

[3] T. Chen and C. Guestrin. XGBoost: A Scalable Tree Boosting System. In *Proc. SIGKDD*, 2016.

[4] J. Couto. Kernel k-means for categorical data. In *Proc. IDA*, 2005.

[5] J. Devlin, M.-W. Chang, K. Lee, and K. Toutanova. Bert: Pre-training of deep bidirectional transformers for language understanding. In *Proc. NAACL-HLT*, 2019.

[6] A. Dosovitskiy, L. Beyer, A. Kolesnikov, D. Weissenborn, X. Zhai, T. Unterthiner, M. Dehghani, M. Minderer, G. Heigold, S. Gelly, J. Uszkoreit, and N. Houlsby. An Image is Worth 16x16 Words: Transformers for Image Recognition at Scale. In *Proc. ICLR*, 2021.

[7] P. I. Frazier. A Tutorial on Bayesian Optimization. 2018. arXiv:1807.02811.

[8] M. A. Gelbart, J. Snoek, and R. P. Adams. Bayesian optimization with unknown constraints. In *Proc. UAI*, 2014.

[9] A. Grattafiori, A. Dubey, A. Jauhri, A. Pandey, A. Kadian, A. Al-Dahle, A. Letman, A. Mathur, A. Schelten, A. Vaughan, A. Yang, A. Fan, A. Goyal, A. Hartshorn, A. Yang, A. Mitra, A. Sravankumar, A. Korenev, A. Hinsvark, A. Rao, A. Zhang, A. Rodriguez, A. Gregerson, A. Spataru, B. Roziere, B. Biron, B. Tang, B. Chern, C. Caucheteux, C. Nayak, C. Bi, C. Marra, C. McConnell, C. Keller, C. Touret, C. Wu, C. Wong, C. C. Ferrer, C. Nikolaidis, D. Allonsius, D. Song, D. Pintz, D. Livshits, D. Wyatt, D. Esiobu, D. Choudhary, D. Mahajan, D. Garcia-Olano, D. Perino, D. Hupkes, E. Lakomkin, E. AlBadawy, E. Lobanova, E. Dinan, E. M. Smith, F. Radenovic, F. Guzmán, F. Zhang, G. Synnaeve, G. Lee, G. L. Anderson, G. Thattai, G. Nail, G. Mialon, G. Pang, G. Cucurell, H. Nguyen, H. Korevaar, H. Xu, H. Touvron, I. Zarov, I. A. Ibarra, I. Kloumann, I. Misra, I. Evtimov, J. Zhang, J. Copet, J. Lee, J. Geffert, J. Vranes, J. Park, J. Mahadeokar, J. Shah, J. van der Linde, J. Billock, J. Hong, J. Lee, J. Fu, J. Chi, J. Huang, J. Liu, J. Wang, J. Yu, J. Bitton, J. Spisak, J. Park, J. Rocca, J. Johnstun, J. Saxe, J. Jia, K. V. Alwala, K. Prasad, K. Upasani, K. Plawiak, K. Li, K. Heafield, K. Stone, K. El-Arini, K. Iyer, K. Malik, K. Chiu, K. Bhalla, K. Lakhotia, L. Rantala-Yeary, L. van der Maaten, L. Chen, L. Tan, L. Jenkins, L. Martin, L. Madaan, L. Malo, L. Blecher, L. Landzaat, L. de Oliveira, M. Muzzi, M. Pasupuleti, M. Singh, M. Paluri, M. Kardas, M. Tsimpoukelli, M. Oldham, M. Rita, M. Pavlova, M. Kambadur, M. Lewis, M. Si, M. K. Singh, M. Hassan, N. Goyal, N. Torabi, N. Bashlykov, N. Bogoychev, N. Chatterji, N. Zhang, O. Duchenne, O. Çelebi, P. Alrassy, P. Zhang, P. Li, P. Vasic, P. Weng, P. Bhargava, P. Dubal, P. Krishnan, P. S. Koura, P. Xu, Q. He, Q. Dong, R. Srinivasan, R. Ganapathy, R. Calderer, R. S. Cabral, R. Stojnic, R. Raileanu, R. Maheswari, R. Girdhar, R. Patel, R. Sauvestre, R. Polidoro, R. Sumbaly, R. Taylor, R. Silva, R. Hou, R. Wang, S. Hosseini, S. Chennabasappa, S. Singh, S. Bell, S. S. Kim, S. Edunov, S. Nie, S. Narang, S. Raparthy, S. Shen, S. Wan, S. Bhosale, S. Zhang, S. Vandenhende, S. Batra, S. Whitman, S. Sootla, S. Collot, S. Gururangan, S. Borodinsky, T. Herman, T. Fowler, T. Sheasha, T. Georgiou, T. Scialom, T. Speckbacher, T. Mihaylov, T. Xiao, U. Karn, V. Goswami, V. Gupta, V. Ramanathan, V. Kerkez, V. Gonguet, V. Do, V. Vogeti, V. Albiero, V. Petrovic, W. Chu, W. Xiong, W. Fu, W. Meers, X. Martinet, X. Wang, X. Wang, X. E. Tan, X. Xia, X. Xie, X. Jia, X. Wang, Y. Goldschlag, Y. Gaur, Y. Babaei, Y. Wen, Y. Song, Y. Zhang, Y. Li, Y. Mao, Z. D. Coudert, Z. Yan, Z. Chen, Z. Papakipos, A. Singh, A. Srivastava, A. Jain, A. Kelsey, A. Shajnfeld, A. Gangidi, A. Victoria, A. Goldstand, A. Menon, A. Sharma, A. Boesenberg, A. Baevski, A. Feinstein, A. Kallet, A. Sangani, A. Teo, A. Yunus, A. Lupu, A. Alvarado, A. Caples, A. Gu, A. Ho, A. Poulton, A. Ryan, A. Ramchandani, A. Dong, A. Franco, A. Goyal, A. Saraf, A. Chowdhury, A. Gabriel, A. Bharambe, A. Eisenman, A. Yazdan, B. James, B. Maurer, B. Leonhardi, B. Huang, B. Loyd, B. D. Paola, B. Paranjape, B. Liu, B. Wu, B. Ni, B. Hancock, B. Wasti, B. Spence, B. Stojkovic, B. Gamido, B. Montalvo, C. Parker, C. Burton, C. Mejia, C. Liu, C. Wang, C. Kim, C. Zhou, C. Hu, C.-H. Chu, C. Cai, C. Tindal, C. Feichtenhofer, C. Gao, D. Civin, D. Beaty, D. Kreymer, D. Li, D. Adkins, D. Xu, D. Testuggine, D. David, D. Parikh, D. Liskovich, D. Foss, D. Wang, D. Le, D. Holland, E. Dowling, E. Jamil, E. Montgomery, E. Presani, E. Hahn, E. Wood, E.-T. Le, E. Brinkman, E. Arcaute, E. Dunbar, E. Smothers, F. Sun, F. Kreuk, F. Tian, F. Kokkinos, F. Ozgenel,

F. Caggioni, F. Kanayet, F. Seide, G. M. Florez, G. Schwarz, G. Badeer, G. Swee, G. Halpern, G. Herman, G. Sizov, Guangyi, Zhang, G. Lakshminarayanan, H. Inan, H. Shojanazeri, H. Zou, H. Wang, H. Zha, H. Habeeb, H. Rudolph, H. Suk, H. Aspegren, H. Goldman, H. Zhan, I. Damlaj, I. Molybog, I. Tufanov, I. Leontiadis, I.-E. Veliche, I. Gat, J. Weissman, J. Geboski, J. Kohli, J. Lam, J. Asher, J.-B. Gaya, J. Marcus, J. Tang, J. Chan, J. Zhen, J. Reizenstein, J. Teboul, J. Zhong, J. Jin, J. Yang, J. Cummings, J. Carvill, J. Shepard, J. McPhie, J. Torres, J. Ginsburg, J. Wang, K. Wu, K. H. U, K. Saxena, K. Khandelwal, K. Zand, K. Matosich, K. Veeraraghavan, K. Michelena, K. Li, K. Jagadeesh, K. Huang, K. Chawla, K. Huang, L. Chen, L. Garg, L. A, L. Silva, L. Bell, L. Zhang, L. Guo, L. Yu, L. Moshkovich, L. Wehrstedt, M. Khabsa, M. Avalani, M. Bhatt, M. Mankus, M. Hasson, M. Lennie, M. Reso, M. Groshev, M. Naumov, M. Lathi, M. Keneally, M. Liu, M. L. Seltzer, M. Valko, M. Restrepo, M. Patel, M. Vyatskov, M. Samvelyan, M. Clark, M. Macey, M. Wang, M. J. Hermoso, M. Metanat, M. Rastegari, M. Bansal, N. Santhanam, N. Parks, N. White, N. Bawa, N. Singhal, N. Egebo, N. Usunier, N. Mehta, N. P. Laptev, N. Dong, N. Cheng, O. Chernoguz, O. Hart, O. Salpekar, O. Kalinli, P. Kent, P. Parekh, P. Saab, P. Balaji, P. Rittner, P. Bontrager, P. Roux, P. Dollar, P. Zvyagina, P. Ratanchandani, P. Yuvraj, Q. Liang, R. Alao, R. Rodriguez, R. Ayub, R. Murthy, R. Nayani, R. Mitra, R. Parthasarathy, R. Li, R. Hogan, R. Battey, R. Wang, R. Howes, R. Rinott, S. Mehta, S. Siby, S. J. Bondu, S. Datta, S. Chugh, S. Hunt, S. Dhillon, S. Sidorov, S. Pan, S. Mahajan, S. Verma, S. Yamamoto, S. Ramaswamy, S. Lindsay, S. Lindsay, S. Feng, S. Lin, S. C. Zha, S. Patil, S. Shankar, S. Zhang, S. Zhang, S. Wang, S. Agarwal, S. Sajuyigbe, S. Chintala, S. Max, S. Chen, S. Kehoe, S. Satterfield, S. Govindaprasad, S. Gupta, S. Deng, S. Cho, S. Virk, S. Subramanian, S. Choudhury, S. Goldman, T. Remez, T. Glaser, T. Best, T. Koehler, T. Robinson, T. Li, T. Zhang, T. Matthews, T. Chou, T. Shaked, V. Vontimitta, V. Ajayi, V. Montanez, V. Mohan, V. S. Kumar, V. Mangla, V. Ionescu, V. Poenaru, V. T. Mihailescu, V. Ivanov, W. Li, W. Wang, W. Jiang, W. Bouaziz, W. Constable, X. Tang, X. Wu, X. Wang, X. Wu, X. Gao, Y. Kleinman, Y. Chen, Y. Hu, Y. Jia, Y. Qi, Y. Li, Y. Zhang, Y. Zhang, Y. Adi, Y. Nam, Yu, Wang, Y. Zhao, Y. Hao, Y. Qian, Y. Li, Y. He, Z. Rait, Z. DeVito, Z. Rosnbrick, Z. Wen, Z. Yang, Z. Zhao, and Z. Ma. The Llama 3 Herd of Models. 2024.

[10] Y. Huang, Y. Cheng, A. Bapna, O. Firat, M. X. Chen, D. Chen, H. Lee, J. Ngiam, Q. V. Le, Y. Wu, and Z. Chen. GPipe: efficient training of giant neural networks using pipeline parallelism. In *Proc. NeurIPS*, 2019.

[11] D. R. Jones, M. Schonlau, and W. J. Welch. Efficient Global Optimization of Expensive Black-Box Functions. *Journal of Global Optimization*, 13(4):455–492, 1998.

[12] J. Kirschner and A. Krause. Information Directed Sampling and Bandits with Heteroscedastic Noise. In *Proc. COLT*, 2018.

[13] O. Kuchaiev, J. Li, H. Nguyen, O. Hrinchuk, R. Leary, B. Ginsburg, S. Kriman, S. Beliaev, V. Lavrukhin, J. Cook, P. Castonguay, M. Popova, J. Huang, and J. M. Cohen. NeMo: a toolkit for building AI applications using Neural Modules. 2019. arXiv:1909.09577.

[14] B. Lei, T. Q. Kirk, A. Bhattacharya, D. Pati, X. Qian, R. Arroyave, and B. K. Mallick. Bayesian optimization with adaptive surrogate models for automated experimental design. *npj Computational Materials*, 7(1):1–12, Dec. 2021.

[15] D. Li, H. Wang, E. Xing, and H. Zhang. AMP: automatically finding model parallel strategies with heterogeneity awareness. In *Proc. NeurIPS*, 2022.

[16] S. Li, Y. Zhao, R. Varma, O. Salpekar, P. Noordhuis, T. Li, A. Paszke, J. Smith, B. Vaughan, P. Damania, and S. Chintala. PyTorch distributed: experiences on accelerating data parallel training. In *Proc. VLDB*, 2020.

[17] S. Li, H. Liu, Z. Bian, J. Fang, H. Huang, Y. Liu, B. Wang, and Y. You. Colossal-AI: A Unified Deep Learning System For Large-Scale Parallel Training. In *Proc. ICPP*, 2023.

[18] S. Li, F. Xue, C. Baranwal, Y. Li, and Y. You. Sequence parallelism: Long sequence training from system perspective. In *Proc. ACL*, 2023.

[19] Z. Lin, Y. Miao, Q. Zhang, F. Yang, Y. Zhu, C. Li, S. Maleki, X. Cao, N. Shang, Y. Yang, W. Xu, M. Yang, L. Zhang, and L. Zhou. nnScaler: constraint-guided parallelization plan generation for deep learning training. In *Proc. OSDI*, 2024.

[20] H. Liu, C. Li, Q. Wu, and Y. J. Lee. Visual instruction tuning. In *Proc. NeurIPS*, 2023.

[21] A. Makarova, I. Usmanova, I. Bogunovic, and A. Krause. Risk-averse Heteroscedastic Bayesian Optimization. In *Proc. NeurIPS*, 2021.

[22] D. Narayanan, A. Harlap, A. Phanishayee, V. Seshadri, N. R. Devanur, G. R. Ganger, P. B. Gibbons, and M. Zaharia. PipeDream: generalized pipeline parallelism for DNN training. In *Proc. SOSP*, 2019.

[23] OpenAI, J. Achiam, S. Adler, S. Agarwal, L. Ahmad, I. Akkaya, F. L. Aleman, D. Almeida, J. Altenschmidt, S. Altman, S. Anadkat, R. Avila, I. Babuschkin, S. Balaji, V. Balcom, P. Baltescu, H. Bao, M. Bavarian, J. Belgum, I. Bello, J. Berdine, G. Bernadett-Shapiro, C. Berner, L. Bogdonoff, O. Boiko, M. Boyd, A.-L. Brakman, G. Brockman, T. Brooks, M. Brundage, K. Button, T. Cai, R. Campbell, A. Cann, B. Carey, C. Carlson, R. Carmichael, B. Chan, C. Chang, F. Chantzis, D. Chen, S. Chen, R. Chen, J. Chen, M. Chen, B. Chess, C. Cho, C. Chu, H. W. Chung, D. Cummings, J. Currier, Y. Dai, C. Decareaux, T. Degry, N. Deutsch, D. Deville, A. Dhar, D. Dohan, S. Dowling, S. Dunning, A. Ecoffet, A. Eleti, T. Eloundou, D. Farhi, L. Fedus, N. Felix, S. P. Fishman, J. Forte, I. Fulford, L. Gao, E. Georges, C. Gibson, V. Goel, T. Gogineni, G. Goh, R. Gontijo-Lopes, J. Gordon, M. Grafstein, S. Gray, R. Greene, J. Gross, S. S. Gu, Y. Guo, C. Hallacy, J. Han, J. Harris, Y. He, M. Heaton, J. Heidecke, C. Hesse, A. Hickey, W. Hickey, P. Hoeschele, B. Houghton, K. Hsu, S. Hu, X. Hu, J. Huizinga, S. Jain, S. Jain, J. Jang, A. Jiang, R. Jiang, H. Jin, D. Jin, S. Jomoto, B. Jonn, H. Jun, T. Kaftan, L. Kaiser, A. Kamali, I. Kanitscheider, N. S. Keskar, T. Khan, L. Kilpatrick, J. W. Kim, C. Kim, Y. Kim, J. H. Kirchner, J. Kiros, M. Knight, D. Kokotajlo, L. Kondraciuk, A. Kondrich, A. Konstantinidis, K. Kosic, G. Krueger, V. Kuo, M. Lampe, I. Lan, T. Lee, J. Leike, J. Leung, D. Levy, C. M. Li, R. Lim, M. Lin, S. Lin, M. Litwin, T. Lopez, R. Lowe, P. Lue, A. Makanju, K. Malfacini, S. Manning, T. Markov, Y. Markovski, B. Martin, K. Mayer, A. Mayne, B. McGrew, S. M. McKinney, C. McLeavey, P. McMillan, J. McNeil, D. Medina, A. Mehta, J. Menick, L. Metz, A. Mishchenko, P. Mishkin, V. Monaco, E. Morikawa, D. Mossing, T. Mu, M. Murati, O. Murk, D. Mély, A. Nair, R. Nakano, R. Nayak, A. Neelakantan, R. Ngo, H. Noh, L. Ouyang, C. O'Keefe, J. Pachocki, A. Paino, J. Palermo, A. Pantuliano, G. Parascandolo, J. Parish, E. Parparita, A. Passos, M. Pavlov, A. Peng, A. Perelman, F. d. A. B. Peres, M. Petrov, H. P. d. O. Pinto, Michael, Pokorny, M. Pokrass, V. H. Pong, T. Powell, A. Power, B. Power, E. Proehl, R. Puri, A. Radford, J. Rae, A. Ramesh, C. Raymond, F. Real, K. Rimbach, C. Ross, B. Rotsted, H. Roussez, N. Ryder, M. Saltarelli, T. Sanders, S. Santurkar, G. Sastry, H. Schmidt, D. Schnurr, J. Schulman, D. Selsam, K. Sheppard, T. Sherbakov, J. Shieh, S. Shoker, P. Shyam, S. Sidor, E. Sigler, M. Simens, J. Sitkin, K. Slama, I. Sohl, B. Sokolowsky, Y. Song, N. Staudacher, F. P. Such, N. Summers, I. Sutskever, J. Tang, N. Tezak, M. B. Thompson, P. Tillet, A. Tootoonchian, E. Tseng, P. Tuggle, N. Turley, J. Tworek, J. F. C. Uribe, A. Vallone, A. Vijayvergiya, C. Voss, C. Wainwright, J. J. Wang, A. Wang, B. Wang, J. Ward, J. Wei, C. J. Weinmann, A. Welihinda, P. Welinder, J. Weng, L. Weng, M. Wiethoff, D. Willner, C. Winter, S. Wolrich, H. Wong, L. Workman, S. Wu, J. Wu, M. Wu, K. Xiao, T. Xu, S. Yoo, K. Yu, Q. Yuan, W. Zaremba, R. Zellers, C. Zhang, M. Zhang, S. Zhao, T. Zheng, J. Zhuang, W. Zhuk, and B. Zoph. GPT-4 Technical Report. 2024. arXiv:2303.08774.

[24] A. Radford, J. W. Kim, C. Hallacy, A. Ramesh, G. Goh, S. Agarwal, G. Sastry, A. Askell, P. Mishkin, J. Clark, G. Krueger, and I. Sutskever. Learning Transferable Visual Models From Natural Language Supervision. In *Proc. ICML*, 2021.

[25] T. Rainforth, A. Foster, D. R. Ivanova, and F. B. Smith. Modern Bayesian Experimental Design. 2023. arXiv:2302.14545.

[26] S. Rajbhandari, J. Rasley, O. Ruwase, and Y. He. ZeRO: memory optimizations toward training trillion parameter models. In *Proc. SC*, 2020.

[27] S. Rajbhandari, C. Li, Z. Yao, M. Zhang, R. Y. Aminabadi, A. A. Awan, J. Rasley, and Y. He. Deepspeed-moe: Advancing mixture-of-experts inference and training to power next-generation ai scale. In *Proc. ICML*, 2022.

[28] J. Rasley, S. Rajbhandari, O. Ruwase, and Y. He. DeepSpeed: System Optimizations Enable Training Deep Learning Models with Over 100 Billion Parameters. In *Proc. SIGKDD*, 2020.

[29] C. E. Rasmussen and C. K. I. Williams. *Gaussian Processes for Machine Learning*. MIT Press, 2006. ISBN 978-0-262-18253-9.

[30] N. Shazeer, A. Mirhoseini, K. Maziarz, A. Davis, Q. Le, G. Hinton, and J. Dean. Outrageously large neural networks: The sparsely-gated mixture-of-experts layer. In *Proc. ICLR*, 2017.

[31] M. Shoeybi, M. Patwary, R. Puri, P. LeGresley, J. Casper, and B. Catanzaro. Megatron-LM: Training Multi-Billion Parameter Language Models Using Model Parallelism. 2020. arXiv:1909.08053.

[32] J. Snoek, H. Larochelle, and R. P. Adams. Practical Bayesian optimization of machine learning algorithms. In *Proc. NeurIPS*, 2012.

[33] N. Srinivas, A. Krause, S. M. Kakade, and M. Seeger. Gaussian Process Optimization in the Bandit Setting: No Regret and Experimental Design. *IEEE Transactions on Information Theory*, 58:3250–3265, 2012.

[34] H. Touvron, L. Martin, K. Stone, P. Albert, A. Almahairi, Y. Babaei, N. Bashlykov, S. Batra, P. Bhargava, S. Bhosale, D. Bikel, L. Blecher, C. C. Ferrer, M. Chen, G. Cucurull, D. Esiobu, J. Fernandes, J. Fu, W. Fu, B. Fuller, C. Gao, V. Goswami, N. Goyal, A. Hartshorn, S. Hosseini, R. Hou, H. Inan, M. Kardas, V. Kerkez, M. Khabsa, I. Kloumann, A. Korenev, P. S. Koura, M.-A. Lachaux, T. Lavril, J. Lee, D. Liskovich, Y. Lu, Y. Mao, X. Martinet, T. Mihaylov, P. Mishra, I. Molybog, Y. Nie, A. Poulton, J. Reizenstein, R. Rungta, K. Saladi, A. Schelten, R. Silva, E. M. Smith, R. Subramanian, X. E. Tan, B. Tang, R. Taylor, A. Williams, J. X. Kuan, P. Xu, Z. Yan, I. Zarov, Y. Zhang, A. Fan, M. Kambadur, S. Narang, A. Rodriguez, R. Stojnic, S. Edunov, and T. Scialom. Llama 2: Open Foundation and Fine-Tuned Chat Models. 2023.

[35] A. Vaswani, N. Shazeer, N. Parmar, J. Uszkoreit, L. Jones, A. N. Gomez, L. Kaiser, and I. Polosukhin. Attention is All you Need. In *Proc. NeurIPS*, 2017.

[36] M. Wagenländer, G. Li, B. Zhao, L. Mai, and P. Pietzuch. Tenplex: Dynamic Parallelism for Deep Learning using Parallelizable Tensor Collections. In *Proc. SOSP*, 2024.

[37] J. T. Wilson, R. Moriconi, F. Hutter, and M. P. Deisenroth. The reparameterization trick for acquisition functions. 2017.

[38] D. Xiong, L. Chen, Y. Jiang, D. Li, S. Wang, and S. Wang. Revisiting the Time Cost Model of AllReduce. 2024. arXiv:2409.04202.

[39] A. Yang, B. Yang, B. Hui, B. Zheng, B. Yu, C. Zhou, C. Li, C. Li, D. Liu, F. Huang, G. Dong, H. Wei, H. Lin, J. Tang, J. Wang, J. Yang, J. Tu, J. Zhang, J. Ma, J. Yang, J. Xu, J. Zhou, J. Bai, J. He, J. Lin, K. Dang, K. Lu, K. Chen, K. Yang, M. Li, M. Xue, N. Ni, P. Zhang, P. Wang, R. Peng, R. Men, R. Gao, R. Lin, S. Wang, S. Bai, S. Tan, T. Zhu, T. Li, T. Liu, W. Ge, X. Deng, X. Zhou, X. Ren, X. Zhang, X. Wei, X. Ren, X. Liu, Y. Fan, Y. Yao, Y. Zhang, Y. Wan, Y. Chu, Y. Liu, Z. Cui, Z. Zhang, Z. Guo, and Z. Fan. Qwen2 Technical Report. 2024.

[40] A. Yang, A. Li, B. Yang, B. Zhang, B. Hui, B. Zheng, B. Yu, C. Gao, C. Huang, C. Lv, C. Zheng, D. Liu, F. Zhou, F. Huang, F. Hu, H. Ge, H. Wei, H. Lin, J. Tang, J. Yang, J. Tu, J. Zhang, J. Yang, J. Yang, J. Zhou, J. Zhou, J. Lin, K. Dang, K. Bao, K. Yang, L. Yu, L. Deng, M. Li, M. Xue, M. Li, P. Zhang, P. Wang, Q. Zhu, R. Men, R. Gao, S. Liu, S. Luo, T. Li, T. Tang, W. Yin, X. Ren, X. Wang, X. Zhang, X. Ren, Y. Fan, Y. Su, Y. Zhang, Y. Zhang, Y. Wan, Y. Liu, Z. Wang, Z. Cui, Z. Zhang, Z. Zhou, and Z. Qiu. Qwen3 Technical Report. 2025.

[41] S. Zhang, L. Diao, C. Wu, Z. Cao, S. Wang, and W. Lin. HAP: SPMD DNN Training on Heterogeneous GPU Clusters with Automated Program Synthesis. In *Proc. EuroSys*, 2024.

[42] Y. Zhang, D. W. Apley, and W. Chen. Bayesian Optimization for Materials Design with Mixed Quantitative and Qualitative Variables. *Scientific Reports*, (1):4924, 2020.

[43] Y. Zhao, A. Gu, R. Varma, L. Luo, C.-C. Huang, M. Xu, L. Wright, H. Shojanazeri, M. Ott, S. Shleifer, A. Desmaison, C. Balioglu, P. Damania, B. Nguyen, G. Chauhan, Y. Hao, A. Mathews, and S. Li. PyTorch FSDP: Experiences on Scaling Fully Sharded Data Parallel. In *Proc. VLDB*, 2023.

[44] L. Zheng, Z. Li, H. Zhang, Y. Zhuang, Z. Chen, Y. Huang, Y. Wang, Y. Xu, D. Zhuo, E. P. Xing, J. E. Gonzalez, and I. Stoica. Alpa: Automating Inter- and Intra-Operator Parallelism for Distributed Deep Learning. In *Proc. OSDI*, 2022.

A Additional Discussion on Parallelism Types

Data parallelism. The most basic type of training parallelism is data parallelism (DP) [16] where a batch of training data is split into shards and distributed among each device. These shards are then fed into the local replicas of the models, before the parameter updates from each device are synchronized. While simple and often the fastest, the naive DP approach requires replicating the model on each device, which takes up additional storage on each node. Several methods have since been proposed to perform DP with sharded models, including the Zero Redundancy Optimizer (ZeRO) introduced by [26] in the DeepSpeed package, and Fully-Sharded Data Parallel (FSDP) introduced by [43]. While these frameworks allow for efficient DP implementations, their effectiveness can still heavily depend on the choice of hyperparameters. For example, ZeRO involves three different stages of optimization which chooses whether the optimizer states, the model gradients or the model parameters are sharded between each GPU. The choice of sharded items affect the amount of data that has to be stored in each GPU and communicated across GPUs which in turn affects the throughput of the training and the memory usage in each GPU.

Tensor parallelism. Another method for scaling operation is tensor parallelism (TP) where individual tensors are sharded across multiple devices, so that the matrix multiplication operations are instead done in a distributed manner, allowing these operations to scale to larger sizes than otherwise that would fit on a single GPU. TP initially involved splitting a tensor along a single dimension [31], however has since also incorporated sharding tensors across multiple dimensions as well [2].

Pipeline parallelism. In pipeline parallelism (PP) [10, 22] we instead partition the model along its execution pipeline with each model partition running synchronously with microbatches of data. The gradients are accumulated for each microbatch and updated at the end of each training step. By sharding the model and training data into smaller chunks, the GPU memory required at any one time becomes lower, allowing for the training of larger models at the cost of more sequential operation rounds and higher cost of communication between each GPU. The tradeoff between training speed and maximum memory usage can be further controlled based on the size of microbatches and the number of model chunks.

B Technical Primer on Gaussian Processes and Bayesian Optimization

In this section, we provide a technical overview of Gaussian process (GP) regression and on Bayesian optimization (BO). The contents are adapted from [7, 29].

A Gaussian process (GP) $\mathcal{GP}(\mu_{\text{prior}}, k)$ with prior mean μ_{prior} and covariance k is a random process where for any subset of input $\mathbf{X}$, its corresponding output is given by a normal distribution $f(\mathbf{X}) \sim \mathcal{N}\big(\mu_{\text{prior}}(\mathbf{X}), k(\mathbf{X}, \mathbf{X})\big)$. The prior mean $\mu_{\text{prior}}(x)$ describes the expected value of the random function $f(x)$ at a certain input, while the prior covariance $k(x, x')$ roughly captures that between $f(x)$ and $f(x')$.

Suppose that we have an unknown function f drawn from the GP. Given a set $D = (\mathbf{X}, \mathbf{y}) = \{(x_1, y_1), \ldots, (x_n, y_n)\}$ of inputs and corresponding measurements, where $y_i = f(x_i) + \epsilon_i$ are noisy measurements of the actual function with Gaussian noise $\epsilon_i \sim \mathcal{N}(0, \lambda_i)$. Then, when performing Bayesian inference, we can express the GP posterior mean and covariance as

$$\mu(x) = \mu_{\text{prior}}(x) + k(x, \mathbf{X})\big(k(\mathbf{X}) + \text{diag}(\lambda)\big)^{-1}(\mathbf{y} - \mu_{\text{prior}}(x)) \,, \tag{4}$$

$$\sigma^2(x) = k(x, x) - k(x, \mathbf{X})\big(k(\mathbf{X}) + \text{diag}(\lambda)\big)^{-1}k(\mathbf{X}, x) \,. \tag{5}$$

In practice, the prior mean and covariance may have hyperparameters θ which specify what functions it is able to model. For example, many kernels representing the prior covariance include lengthscale values, which govern how correlated the function output is when a certain input dimension changes. One method to find the optimal hyperparameters for the kernel is by finding the hyperparameters which maximize the marginal log-likelihood.

In Bayesian optimization (BO), the goal is to find the maxima of the unknown function f. This function is black-box with no analytical form. To do so, we can learn more about f by querying it at different inputs, and perform Bayesian inference to update our belief on the unknown function.

Given the measurements $\mathcal{D}_t = (\mathbf{X}_t, \mathbf{y}_t) = \{(x_1, y_1), \ldots, (x_t, y_t)\}$ in round t of data selection, GP regression can be performed to obtain a posterior mean μ_t and variance σ_t^2. The next input to query x_{t+1} can be chosen as the input which maximizes some acquisition function. Examples of such acquisition function include the expected improvement [11]

$$\mathrm{EI}_t(x) = \mathbb{E}_{y' \sim \mathcal{N}(\mu_{t-1}(x), \sigma_{t-1}^2(x))}\big[\max(0, y' - \max_{y \in \mathbf{y}_{t-1}} y)\big] \tag{6}$$

or the upper confidence bound [33]

$$\mathrm{UCB}_t(x) = \mu_{t-1}(x) + \beta_t \sigma_{t-1}(x) \tag{7}$$

where $\beta_t > 0$ is a constant that may vary with t. In all of these acquisition functions, a tradeoff is performed between selecting inputs that the GP is uncertain about (i.e., with high $\sigma_{t-1}^2(x)$) to learn more about those unknown region, and selecting inputs in regions where the function value is known to be higher (i.e., with high $\mu_{t-1}(x)$).

C Detailed Discussion on Problem Setting

C.1 Hyperparameters Considered

In Table 1, we list several hyperparameters which we include in our parallelism configuration and the range of the values. Note that the hyperparameters are constrained to give a valid PC as well; for example, we ensure that $\texttt{dp} \cdot \texttt{tp} \cdot \texttt{pp} = \texttt{n\_gpus}$ to ensure that each dimension do not exceed number of GPUs. Some hyperparameters are also set to their default value when not in use; for example, if $\texttt{pp} = 1$ (i.e., no PP used) then we restrict $\texttt{mb} = \texttt{mc} = 1$ such that PCs are not duplicated. In the code, we generate all possible PCs beforehand so we can ensure that all PCs chosen will be valid according to the constraints.

Table 1: Tunable hyperparameters in a parallelism configuration.

Hyperparameter	Description	Feasible Values	Notes
DP size (`dp`)	Data parallelism degree	[1, `n_gpus`]	
TP size (`tp`)	Tensor parallelism degree	[1, `n_gpus`]	Requires $\texttt{dp} \cdot \texttt{tp} \cdot \texttt{pp} = \texttt{n\_gpus}$
PP size (`pp`)	Pipeline parallelism degree	[1, `n_gpus`]	
SP size	Sequence parallelism degree	[1, `n_gpus`]	Only NeMo and must be $\leq$ `tp`
CP size	Context parallelism degree	[1, `n_gpus`]	Only NeMo and only for some experiments
EP size	Expert parallelism degree	[1, `n_gpus`]	Only NeMo and only for MoE
DP bucket size	Size for gradient reduction buckets (MB)	[1, 4096]	Only Colossal-AI
ZeRO stage	ZeRO stage used	[0, 3]	For Colossal-AI, must be ≤ 2 For NeMo, this controls FSDP sharding instead
ZeRO bucket size	Bucket size for ZeRO communication	[1, 4096]	
Overlap ZeRO communication	Whether to overlap ZeRO communication	True / False	
Overlap DP AllGather	Whether to overlap AllGather	True / False	
# microbatches (`mb`)	Number of microbatches per forward pass	$\leq$ batch size	Only considered for Colossal-AI
# model chunks (`mc`)	Number of model chunks for pipelining	$\leq$ # transformer blocks	
Overlap P2P for PP	Overlap PP communication or not	True / False	
Grad. checkpointing	Whether gradient checkpointing is enabled	True / False	

C.2 Throughput vs. Time Per Training Step

We explain why we choose to maximize throughput instead of minimizing time per training step.

As an example, suppose we consider three PCs H, H', H'' where the times per training step are given by $\mathcal{T}(H) = 0.3$, $\mathcal{T}(H') = 0.4$, and $\mathcal{T}(H'') = 0.5$. In this case, H would be the best PC out of the three. We see here the gap of the time per training step between H and H' is $\mathcal{T}(H') - \mathcal{T}(H) = 0.1$, and the same gap size for H' and H'' of $\mathcal{T}(H'') - \mathcal{T}(H') = 0.1$. Meanwhile, the gap between the throughput of the two PCs would be $\mathcal{R}(H) - \mathcal{R}(H') = \mathcal{T}(H)^{-1} - \mathcal{T}(H')^{-1} = 3.\overline{3} - 2.5 = 0.8\overline{3}$ and $\mathcal{R}(H') - \mathcal{R}(H'') = \mathcal{T}(H)^{-1} - \mathcal{T}(H')^{-1} = 2.5 - 2 = 0.5$. We can see that the gap between the best PC becomes enhanced when we consider the throughput, when we compare it with the relative gap size of the training step time.

More concretely, if we have a PC which requires time t per training step, then you can reduce it by an amount of Δt, then the throughput would have increased by an amount $(\Delta t)/t^2$. When t becomes smaller, the change in throughput will also increase but at an increasing rate. This therefore means by modeling the throughput, the scores of the good PCs will be more clearly separated.

Additionally, we also consider a maximization of throughput since throughput would be bounded by $[0, r_{\text{max}}]$, rather than the time per training step which would be unbounded on one end, i.e., be in the

interval $[t_{\min}, \infty)$ which makes suboptimal PCs easier to handle. Also, we frame our problem as a maximization in order to be consistent with Bayesian optimization works which typically considers a maximization problem.

D Detailed Discussion of Surrogate Models used by OPPA

D.1 Domain Knowledge

In this section, we elaborate on how the throughput prior mean is constructed in order to obtain the form for the parallelism-informed prior mean. In summary, we design the prior to incorporate the following characteristics.

- *Parallelism coverage.* We model DP/TP traffic via All-Reduce–style collectives and PP via point-to-point transfers, using a placement-aware split of intra- and inter-node links. For computation costs, we also explicitly consider the pipeline bubbles.
- *Topology and protocol awareness.* The communication term uses canonical ring/tree scaling with hierarchical aggregation (node-local first, then cross-node), while collapsing ZERO stages into a single All-Reduce operation at the bandwidth level (bytes over the wire are of the same order) and letting stage-specific latency/overlap differences be absorbed by $\mathbf{C}$ (e.g., event counts, bucket sizes, communication overhead for each parallelism dimension, etc.).
- *Hardware agnosticism via learning.* Rather than hard-coding device/network constants, we expose a small set of effective coefficients that are learned from a few traces. This keeps the prior portable across models, data types, and interconnects while preserving the correct asymptotic trends for `dp`, `tp`, and `pp`.

To predict the computation time, we assume an idealized machine with infinitely many processors such that DP and TP can be perfectly parallelized. Meanwhile, PP using an interleaved schedule incurs additional computation time from the microbatches being ran sequentially, and from pipeline bubble when the first microbatch is being fed through the pipeline [22]. This additional computation time from PP, visualized in Fig. 10, is roughly equal to

$$\widehat{T}_{\text{comp}}(H; t_{\text{comp}}) = \frac{t_{\text{comp}}}{\texttt{n\_gpus}} \cdot \left(\texttt{mb} + \frac{\texttt{pp} - 1}{\texttt{mc}} \right) \tag{8}$$

where `mb` is the number of microbatches used in PP (set to 1 when PP is not used), `mc` is the number of model chunks for PP (also set to 1 when PP is not used), and $t_c = t_f + t_b$ is the total time to perform the forward and backward passes.

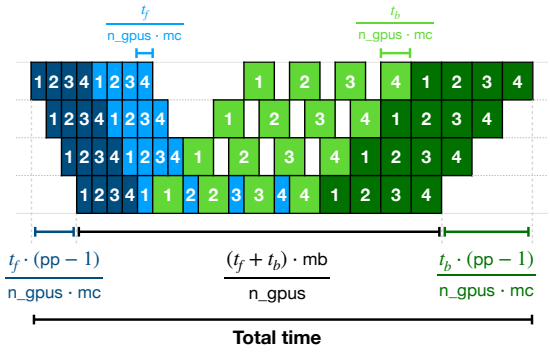

Figure 10: Predicted computation time for PP where t_f and t_b are the time required for the forward and backward stages respectively, for when $\texttt{pp} = \texttt{n\_gpus} = 4$, $\texttt{mb} = 4$, and $\texttt{mc} = 2$

To predict the communication time, inspired by the model visualized in Fig. 2, we assume that DP and TP involve All-Reduce communications and PP P2P communications, where all these costs are modeled separately. We use an extended (α, β, γ) model discussed in [38], and for the intra- and inter-node communications, we characterize the network performance by the latency α_{intra} and α_{inter},

the per-byte bandwidth cost β_{intra} and β_{inter}, the incast overhead γ_{intra} and γ_{inter}, and the memory access overhead δ_{intra} and δ_{inter}. We assume that the inter-node communication costs will be larger than their intra-node counterparts.

For DP and TP, we assume that the Ring All-Reduce implementation is used where the cost to gather and scatter data of size N across D GPUs is given by

$$C_{\text{AR}}(D, N, \alpha, \beta, \gamma, \delta) = 2(D-1)\alpha + \frac{D-1}{D} N(2\beta + \gamma + 3\delta). \tag{9}$$

For DP, we consider the gradient synchronization from the All-Reduce procedure. The data size per GPU for DP All-Reduce, $N_{\texttt{dp}}$, is

$$N_{\texttt{dp}} = \lambda_Z \frac{M_{\text{model}}}{\texttt{tp} \cdot \texttt{pp}} \tag{10}$$

where M_{model} is a learnable total model parameter size, and λ_Z is a tiny fudge for ZERO flavor while staying in AR-land, and it accounts for param-All-Gather + grad-Reduce-Scatter volume equivalence with small overhead for ZERO-3.

Suppose G_{node} is the number of GPUs per node. The overall communication cost from DP $\widehat{\mathcal{T}}_{\text{comm,dp}}$ would then depend on the configuration of the network as follows:

- In a **hierarchical** (multi-node scenario with $\texttt{dp} > G_{\text{node}}$) system, the cost is given by

$$\begin{aligned}\widehat{\mathcal{T}}_{\text{comm,dp}}(H; \mathbf{C}) = {} & C_{\text{AR}}(G_{\text{node}}, N_{\texttt{dp}}, \alpha_{\text{intra}}, \beta_{\text{intra}}, \gamma_{\text{intra}}, \delta_{\text{intra}}) \\ & + C_{\text{AR}}(\lceil \texttt{dp}/G_{\text{node}} \rceil, N_{\texttt{dp}}/G_{\text{node}}, \alpha_{\text{inter}}, \beta_{\text{inter}}, \gamma_{\text{inter}}, \delta_{\text{inter}}).\end{aligned} \tag{11}$$

- In a **flat inter-node** (multi-node scenario with $\texttt{dp} \leq G_{\text{node}}$), the cost is given by

$$\widehat{\mathcal{T}}_{\text{comm,dp}}(H; \mathbf{C}) = C_{\text{AR}}(\texttt{dp}, N_{\texttt{dp}}, \alpha_{\text{inter}}, \beta_{\text{inter}}, \gamma_{\text{inter}}, \delta_{\text{inter}}). \tag{12}$$

- In a **flat intra-node** (single-node scenario), the cost is given by

$$\widehat{\mathcal{T}}_{\text{comm,dp}}(H; \mathbf{C}) = C_{\text{AR}}(\texttt{dp}, N_{\texttt{dp}}, \alpha_{\text{intra}}, \beta_{\text{intra}}, \gamma_{\text{intra}}, \delta_{\text{intra}}). \tag{13}$$

Depending on the hardware used, the appropriate cost for the scenario can be selected.

For TP, we consider the cost from frequent activation communication (e.g., All-Reduce per layer). Let $M_{\text{act,tp}}$ be a learnable characteristic data size for one such TP All-Reduce operation. Let $O_{\texttt{tp/mb}}$ be the learnable number of these operations per microbatch. The total number of TP communication operations is $N_{\texttt{tp,ops}} = O_{\texttt{tp/mb}} \cdot \texttt{mb}$, and the cost of a single TP All-Reduce operation is $C_{\text{AR}}(\texttt{tp}, M_{\text{act,tp}}, \alpha_{\text{eff}}, \beta_{\text{eff}}, \gamma_{\text{eff}}, \delta_{\text{eff}})$ where effective parameters $\alpha_{\text{eff}}, \beta_{\text{eff}}, \gamma_{\text{eff}}, \delta_{\text{eff}}$ are chosen as intra-node or inter-node based on whether the tp group spans multiple nodes (i.e., if $N_H > 1$ and $\texttt{tp} > G_{\text{node}}$) or not. Then, the total TP communication cost is the number of communication operations multiplied by the cost per communication operation, or

$$\widehat{\mathcal{T}}_{\text{comm,tp}}(H; \mathbf{C}) = N_{\texttt{tp,ops}} \cdot C_{\text{AR}}(\texttt{tp}, M_{\text{act,tp}}, \alpha_{\text{eff}}, \beta_{\text{eff}}, \gamma_{\text{eff}}, \delta_{\text{eff}}). \tag{14}$$

For PP, we consider the point-to-point (P2P) transfers of activations and gradients between pp pipeline stages where the cost to transfer data of size N is given by

$$C_{\text{P2P}}(N, \alpha, \beta) = \alpha + N \cdot \beta. \tag{15}$$

Let $M_{\text{act,pp}}$ be a learnable characteristic data size for one P2P transfer (e.g., the size of an activation tensor). The number of communication boundaries is $\texttt{pp} - 1$. Communication occurs for each of mb microbatch, in both forward (activations) and backward (gradients) directions. The total number of P2P communications is given by $N_{\text{pp,transfers}} = \max(\texttt{pp} - 1, 0) \cdot 2\texttt{mb}$ where a single P2P transfer uses effective latency α_{eff} and effective per-unit-data cost $\beta_{\text{pp,eff}}$ (derived from base β parameters), chosen as intra-node or inter-node based on whether communicating stages are on different nodes (approximated if $N_H > 1$). Given this, the overall cost of all communications related to PP would be given by

$$\widehat{\mathcal{T}}_{\text{comm,pp}}(H; \mathbf{C}) = N_{\text{pp,transfers}} \cdot C_{\text{P2P}}(M_{\text{act,pp}}, \alpha_{\text{eff}}, \beta_{\text{pp,eff}}). \tag{16}$$

Here, if $\texttt{pp} = 1$, then $\widehat{\mathcal{T}}_{\text{comm,pp}} = 0$.

When combining the communication costs for all three types of parallelism, considering in practice large chunks of communication overlap with compute, we attach non-overlap factors κ and obtain

$$\widehat{\mathcal{T}}_{\text{comm}}(H;\mathbf{C}) = \kappa_{\texttt{dp}} \cdot \widehat{\mathcal{T}}_{\text{comm},\texttt{dp}}(H;\mathbf{C}) + \kappa_{\texttt{tp}} \cdot \widehat{\mathcal{T}}_{\text{comm},\texttt{tp}}(H;\mathbf{C}) + \kappa_{\texttt{pp}} \cdot \widehat{\mathcal{T}}_{\text{comm},\texttt{pp}}(H;\mathbf{C}) \tag{17}$$

where $\mathbf{C}$ are constants related to the various costs which are to be inferred. Given (8) and (17), we can construct the prior mean for throughput to be

$$\widehat{\mathcal{R}}(H;\{t_{\text{comp}},\mathbf{C}\}) = \left[\widehat{\mathcal{T}}_{\text{comp}}(H;t_{\text{c}}) + \widehat{\mathcal{T}}_{\text{comm}}(H;\mathbf{C})\right]^{-1}. \tag{18}$$

D.2 Parallelism-Informed Prior Mean for the Maximum Memory Usage

We briefly elaborate on the choice of prior mean in (19). As discussed, we only consider the memory that is required to store the NN parameters, and those to compute the gradient updates.

For NN parameters, its sharding can be done on the pipeline or on the layers, allowing us to approximate the GPU memory required for storing the NN parameters to be inversely proportional to $\texttt{pp}\cdot\texttt{tp}$. Note that assuming the simplest DP implementation, the NN parameters are duplicated and stored on each DP dimension, and so the maximum memory usage is not affected by the DP.

Meanwhile, in the case of backpropagation computation, the maximum memory used will roughly be proportional to how many model parameters a certain GPU has to perform the forward and backward passes for, times how many training samples the GPU has to process at any one time. We expect this quantity to be inversely proportional to the number of total GPUs times the latter to depend on the number of microbatches used.

Combining these two factors, can write the maximum memory usage as

$$\widehat{\mathcal{M}}(H;\theta_{\mathcal{M}}) = \min\left\{m_1\cdot(\texttt{pp}\cdot\texttt{tp})^{-1} + m_2\cdot(\texttt{n\_gpus}\cdot\texttt{mb})^{-1} + m_3,\ M_0\right\} \tag{19}$$

where, m_1 captures the memory used for storing model parameters, and m_2 captures the memory used during backpropagation computations, m_3 are any other additional memory overheads unaccounted for by our model, and $\theta_{\mathcal{M}} = \{m_1, m_2, m_3\}$. Note that since we cannot measure maximum memory usage above values of M_0, we apply the $\min$ function to clip the GP prior beliefs.

D.3 Kernel for Modelling the Unknown Deviations

Given the embedding $e(H)$, we use the Matern kernel [29] which is given by

$$k(H,H') = \sigma_k^2 k_{\text{Matern},\nu}\big(e(H),e(H');\ell\big) = \sigma_k^2\frac{2^{1-\nu}}{\Gamma(\nu)}\big(\sqrt{2\nu}\,d_\ell(H,H')\big)^\nu K_\nu\big(\sqrt{2\nu}\,d_\ell(H,H')\big)$$

where Γ is the Gamma function, K_ν is the modified Bessel function, σ_k is the kernel scaling constant,

$$d_\ell(H,H') = \big(e(H)-e(H')\big)^\top\mathbf{L}^{-2}\big(e(H)-e(H')\big) \tag{20}$$

is the distance between two PC embeddings and $\mathbf{L} = \text{diag}(\ell) = \text{diag}([\,\ell_1\cdots\ell_p\,])$ is the lengthscale.

Justification for kernel based on Euclidean distance. Note that in our setup, we use a kernel based on the Euclidean distance despite a discrete search space. This is because we expect each value within the PCs are typically correlated according to its order (e.g., throughput when $\texttt{dp}=1$ will correlate with when $\texttt{dp}=2$, which then correlates with when $\texttt{dp}=4$, etc.). In this regard, there exists some correlation between PCs that have similar values under our embedding (even if the values are all discrete), justifying our use of GPs.

We also observe this later in Table 6 which shows that the lengthscales learned by the GP are larger in some values even without explicit treatment of the discrete values, suggesting existence of learned interpolations by OPPA. Additionally, later in Fig. 20, we demonstrate that OPPA which uses a Matern kernel outperforms OPPA which instead uses a categorical based on the Hamming distance as in [4], which empirically further justifies our kernel choice.

D.4 GP Posterior Beliefs of Throughput and Maximum Memory Usage

Suppose we are in the ith round. We let $\mathbf{H}_i = [H_1\cdots H_i]$ be the list of PCs, $\bar{\mathbf{r}}_i = [\bar{r}_{1,\hat{q}_1}\cdots\bar{r}_{i,\hat{q}_i}]$ and $\sigma^2_{\bar{\mathbf{r}}_i} = [\sigma^2_{\bar{r}_{1,\hat{q}_1}}\cdots\sigma^2_{\bar{r}_{i,\hat{q}_i}}]$ be the measured throughput and the corresponding variance, and $\mathbf{m}_i = [m_1\cdots m_i]$ be the measured maximum memory usage values.

Given the data, we first find the optimal hyperaparameters $\theta = \{\theta_{\mathcal{R}}, \theta_{\mathcal{M}}, \theta_k\}$. This is done by maximizing the marginal log-likelihood [29], or

$$\theta = \arg\max_{\theta'} \ \log p(\bar{\mathbf{r}}_i, \bar{\mathbf{m}}_i | \bar{\mathbf{H}}_i, \theta). \tag{21}$$

The GP posterior beliefs of the throughput and maximum memory usage for any PC H' are then given by normal distributions

$$\mathcal{N}\big(\mu_{\mathcal{R},i}(H'), \sigma^2_{\mathcal{R},i}(H')\big) \quad \text{and} \quad \mathcal{N}\big(\mu_{\mathcal{M},i}(H'), \sigma^2_{\mathcal{M},i}(H')\big) \tag{22}$$

where the mean and variance for the throughput for any PC H' can then be defined as

$$\mu_{\mathcal{R},i}(H') = \widehat{\mathcal{R}}(\mathbf{H}_i; \theta_{\mathcal{R}}) + k(H', \mathbf{H}_i; \theta_k)\big(k(\mathbf{H}_i, \mathbf{H}_i; \theta_k) + \text{diag}(\sigma^2_{\bar{\mathbf{r}}_i})\big)^{-1}\big(\bar{\mathbf{r}}_i - \widehat{\mathcal{R}}(\mathbf{H}_i; \theta_{\mathcal{R}})\big), \tag{23}$$

$$\sigma^2_{\mathcal{R},i}(H') = k(H', H'; \theta_k) - k(H', \mathbf{H}_i; \theta_k)\big(k(\mathbf{H}_i, \mathbf{H}_i; \theta_k) + \text{diag}(\sigma^2_{\bar{\mathbf{r}}_i})\big)^{-1} k(\mathbf{H}_i, H'; \theta_k), \tag{24}$$

and the GP posterior mean and variance for the memory usage for any PC H' can then be defined as

$$\mu_{\mathcal{M},i}(H') = \widehat{\mathcal{M}}(\mathbf{H}_i; \theta_{\mathcal{M}}) + k(H', \mathbf{H}_i; \theta_k)\big(k(\mathbf{H}_i, \mathbf{H}_i; \theta_k) + \lambda I\big)^{-1}\big(\mathbf{m}_i - \widehat{\mathcal{M}}(\mathbf{H}_i; \theta_{\mathcal{M}})\big), \tag{25}$$

$$\sigma^2_{\mathcal{M},i}(H') = k(H', H'; \theta_k) - k(H', \mathbf{H}_i; \theta_k)\big(k(\mathbf{H}_i, \mathbf{H}_i; \theta_k) + \lambda I\big)^{-1} k(\mathbf{H}_i, H'; \theta_k) \tag{26}$$

where λ is to make the matrix invertible.

E Detailed Discussion of PC Selection Method in OPPA

E.1 Constrained UCB Criterion

The next PC $H_i \in \mathcal{H}$ to trial in round i is chosen to be the PC which maximizes the constrained upper confidence bound (cUCB) [33, 37], given by

$$\text{cUCB}_i(H) \triangleq \mathbb{E}_{\hat{r}_{H,i-1}, \hat{m}_{H,i-1}}\big[X_{H,i-1} + \beta_i \big| X_{H,i-1} - \mathbb{E}[X_{H,i-1}]\big|\big] \tag{27}$$

where $\hat{r}_{H,i-1} \sim \mathcal{N}\big(\mu_{\mathcal{R},i-1}(H), \sigma^2_{\mathcal{R},i-1}(H)\big)$ and $\hat{m}_{H,i-1} \sim \mathcal{N}\big(\mu_{\mathcal{M},i-1}(H), \sigma^2_{\mathcal{M},i-1}(H)\big)$ are sampled from their respective GPs as modeled from ①, and $X_{H,i-1} = \hat{r}_{H,i-1} \cdot \big(1 - \texttt{sigmoid}(\hat{m}_{H,i-1})\big)$. Note that in the case that memory constraint is not violated (i.e., when $\texttt{sigmoid}(\hat{m}_{H,i-1}) \approx 0$), the objective in (27) can be reduced to the analytical UCB objective (i.e., $\text{cUCB}_i(H) \approx \mu_{\mathcal{R},i-1}(H) + \beta_i \sigma_{\mathcal{R},i-1}(H)$).

E.2 Random Sampling For Additional Exploration

In OPPA, we sometimes select PCs at random for additional exploration. There are two scenarios which triggers a random selection of PC in OPPA.

1. In the first few chosen PCs. This is because in the beginning there are no PCs which can be used to infer the hyperparameters for the prior distribution of the GP, therefore a few PCs are chosen at random to kick-off the modeling process and provide a reasonably diverse set of samples to infer the hyperparameters well.
2. When too many out-of-memory errors have been encountered in a row. This is because any out-of-memory trials will not result in a usable training data for the throughput modeling and possibly minimal data for the maximum memory GP which does not aid the GP model. When too many such cases are encountered, we attempt to do random exploration so that the model can receive some information that can be used to model better with and find new feasible PCs.

For the random selection process, we select a PC using a weighted random strategy, where we first select a parallelism dimension configuration uniformly at random, then select the remaining hyperparameters uniformly at random such that they are feasible within the selected parallelism dimension configuration.

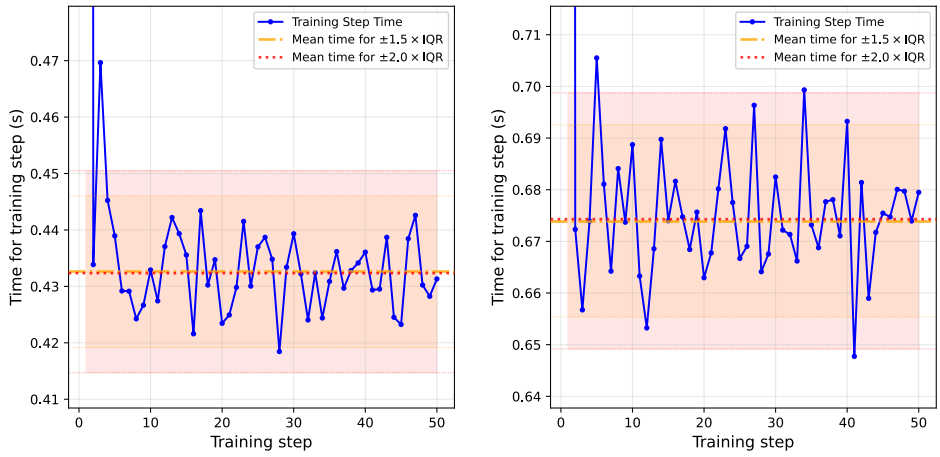

Figure 11: Example of the outlier removal process based on the IQR on different random PC trials. Here, we show the effect of the threshold selected vs. the mean of the measurements, demonstrating the robustness with respect to the different thresholds.

F Detailed Discussion of PC Trialing Method

F.1 Throughput Estimation

Given the time $t_{i,1}, \ldots, t_{i,q}$ required for q training steps, we can estimate the throughput and its predicted variance as

$$\bar{r}_{i,q} = \frac{1}{q}\sum_{j=1}^{q}\frac{1}{t_{i,j}}, \quad \text{and} \quad \sigma^2_{\bar{r}_{i,q}} = \frac{1}{q}\sum_{j=1}^{q}\left(\frac{1}{t_{i,j}} - \bar{r}_{i,q}\right)^2. \tag{28}$$

Note that $\bar{r}_{i,q}$ can be viewed as an unbiased estimator of the reciprocal of the time per training step (i.e., $\mathbb{E}[\bar{r}_{i,q}] = 1/\mathcal{T}(H_i)$ where $\mathcal{T}(H_i)$ is the average time per training step), while $\sigma^2_{\bar{r}_{i,q}}$ is the variance of the estimator.

F.2 Outlier Removal

As demonstrated in Fig. 3, not all training time measurements will be representative of the actual throughput. We therefore perform two actions. First, we remove the first training step $t_{i,1}$ since it typically corresponds to a warm-up for the training and therefore will usually be an anomaly measurement. Second, we compute the median and the inter-quartile range (IQR), and remove all measurements which are away from the median by at least $2 \times IQR$. This is a standard method for outlier removal in practice. However, we choose a looser threshold for outliers to account for fluctuating measurements. This generally has little effect on the overall optimization since most training steps tend to not fluctuate by too much anyway. This is demonstrated by Fig. 11 which shows that the predicted throughput would have little difference across the threshold of outlier removal, showing robustness of our method to the outlier removal process. The remaining training points are then used to compute (28).

F.3 Additional Discussion on Early Trial Termination Mechanism

In this section, we attempt to prove Thm. 4.1. To do so, we will consider a more general case for an arbitrary unknown function f. We do so since the problem setting of sequential repeated measurements is useful in many problem settings beyond optimizing the PC, such as in repeated scientific experiments where we can decide on-the-fly whether the same experimental setup should be repeated or not. We will first provide an intuitive justification for why early termination can be applied, followed by a theoretical proof for Thm. 4.1 and ablation studies on synthetic functions.

F.3.1 Intuition Behind Early Termination Mechanism

Before stating the formal proof, we provide some intuition behind why the early termination mechanism saves on resources while also not affecting the overall performance. In Fig. 12, we present a toy example of a BO iteration where an input is repeatedly queried.

Here, we notice several things. We first see that for a certain input, more repetitions of the query will result in a lower standard deviation for the measurement. This is simply from the fact that when we take the mean of several i.i.d. measurements, the mean will tend towards the actual value, and the variance of the mean predictor will decay at a rate inversely proportional to the number of repeated measurements. This is reflected in the plots where the measurement at $x = 2$ has smaller and smaller standard deviation as we have more repeats, and as we will show in Corollary F.2. In these cases, we see that some repeated queries are therefore necessary to reduce the noise of the measurements.

However, as we perform more repeats, there is a diminishing effect on how much more information is gained from each additional repeats. In the diagram, we see that after 20 repeated measurements (as in Fig. 12c), the GP would barely change. Similarly, we see that at 20 repeats, we are able to somewhat conclude that the global optimum is less likely to be in the neighborhood of $x = 2$, as reflected by the corresponding probability density function, and that this belief remains when we continue up to 100 repeats (as in Fig. 12d). This shows the additional repeats are unlikely to improve the predictions by the GP and the confidence of the optimum. We therefore can see that by stopping after 20 repeats, we would have been able to eventually make the same conclusion about the optimum in the end while saving on resources that would have been incurred from repeated queries.

Finally, we note that additional repeats are more beneficial to recovering the optimum value in the case that it improves upon the best measurement so far. In Fig. 13, we see that additional repeated measurements at $x = 2$ eventually results in diminishing returns, as seen in the probability distribution of the maximum value of $f(x)$ being similar between using 20 repeats and 100 repeats. Meanwhile, in Fig. 14 where we instead repeatedly query the input $x = 4.2$, we continue to gain information about the maximum value even when we use 100 repeats, as seen by the sharper probability distribution for the belief of the maximum $f(x)$. We therefore can see that additional repeats are less informative if they are for suboptimal inputs. We can therefore use this idea to form a metric to determine if a trial should be terminated early.

F.3.2 Proof of Thm. 4.1

With this intuition, we will now formally prove the performance of the early termination mechanism. For completeness, we first state the assumptions for the function and the measurements which follow from other BO works [12, 21, 33] however with additional assumptions on repeated measurements from the same input.

Assumption F.1. Let $f \sim \mathcal{GP}(0, k)$ be an unknown function whose RKHS norm $\|f\|_{\mathcal{H}} \leq B$ is bounded. The BO algorithm is as noted in Algorithm 3, where in each BO iteration i, an input $x_i \in \mathcal{X}$ is selected, and $\hat{q}_i \leq q_{\max}$ noisy outputs $y_{i,j} = f(x_i) + \varepsilon_{i,j}$ are returned, where $\varepsilon_{i,j} \sim \mathcal{N}(0, s^2)$ are i.i.d. noise.

Note that in this following proof, we consider any function f which has a bounded RKHS norm. While this property also applies for the unknown throughput $\mathcal{R}$, it will also be satisfied by other black-box functions in general as well.

We now also show Algorithm 2 which repeats each query $q_{\max}$ times, and our proposed Algorithm 3 which does early termination on some of the rounds. Our theoretical results in this section will consider Algorithm 3.

We first state a result regarding the mean estimator of $f(x_i)$.

Corollary F.2. *Suppose we define*

$$\bar{y}_{i,q} = \frac{1}{q} \sum_{j=1}^{q} y_{i,j}. \tag{29}$$

Then, the expected value of $\bar{x}_i$ is $\mathbb{E}[\bar{y}_{i,q}] = f(x_i)$, and its variance bounded by $\mathbb{V}[\bar{y}_{i,q}] = s^2/q$.

Proof. The results are direct consequences of the summation of expected values and variances of independent random variables, and the fact that $\mathbb{V}[y_{i,j}] = s^2$ by assumption. □

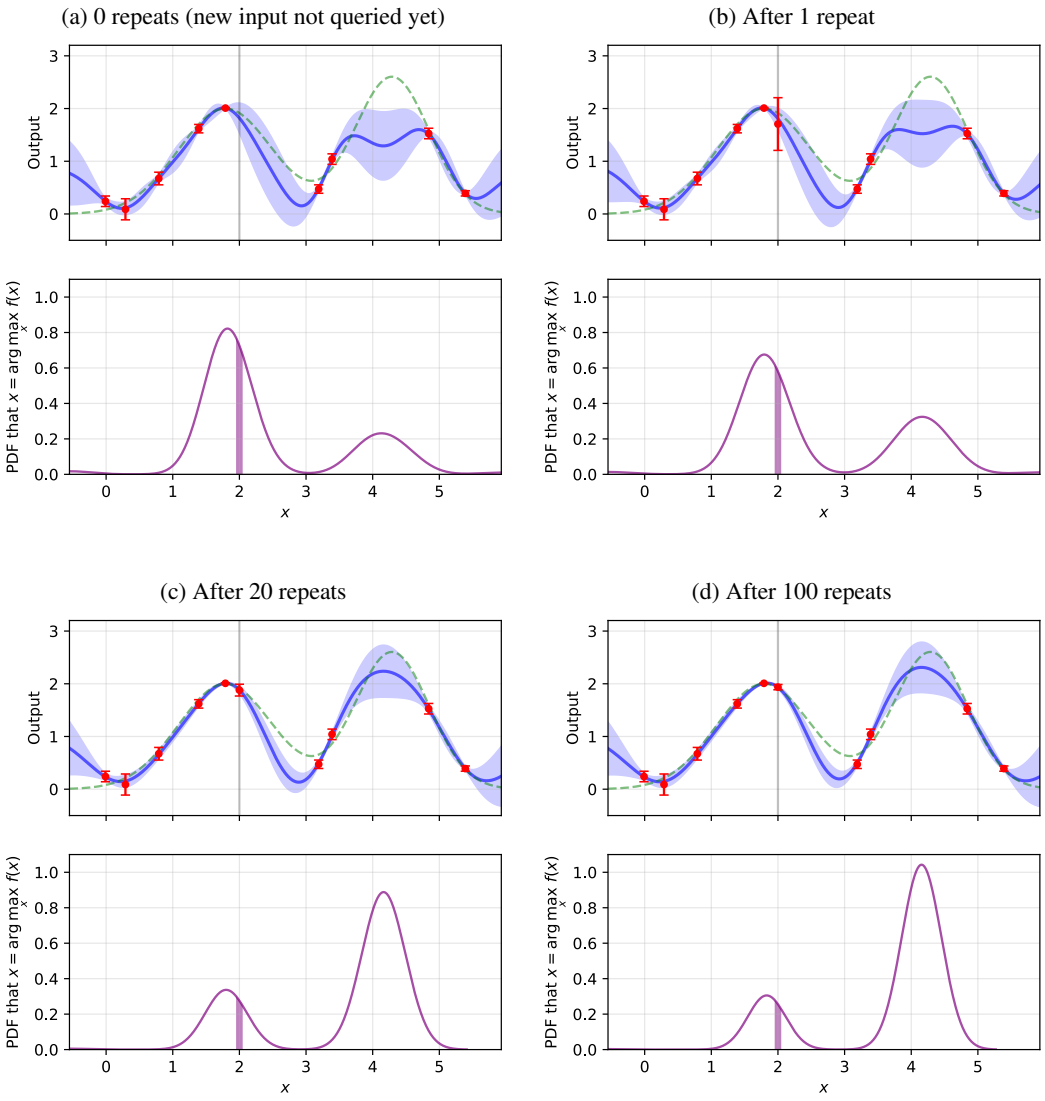

Figure 12: Demonstration of why early termination of certain trials does not affect final result. Figs. 12a to 12d represent the modeled GP and the predicted optimum when a certain input, in this case at $x = \arg\max_{x'} \mu_t(x') + \beta_t \sigma_t(x') = 2$, is repeatedly queried for 0, 1, 20, and 100 times. For each subfigure, the top diagram represents the modeled GP where the dashed green line represents the actual function, the blue line and error band represent the GP mean and standard deviation, and the red points represent the predicted mean and standard deviation (the latter which shrinks with more repeats). In the bottom diagram, we show the probability of each input being the optimal (i.e., probability that $x = \arg\max_{x'} f(x')$), while highlighting the interval around the input $x = 2$.

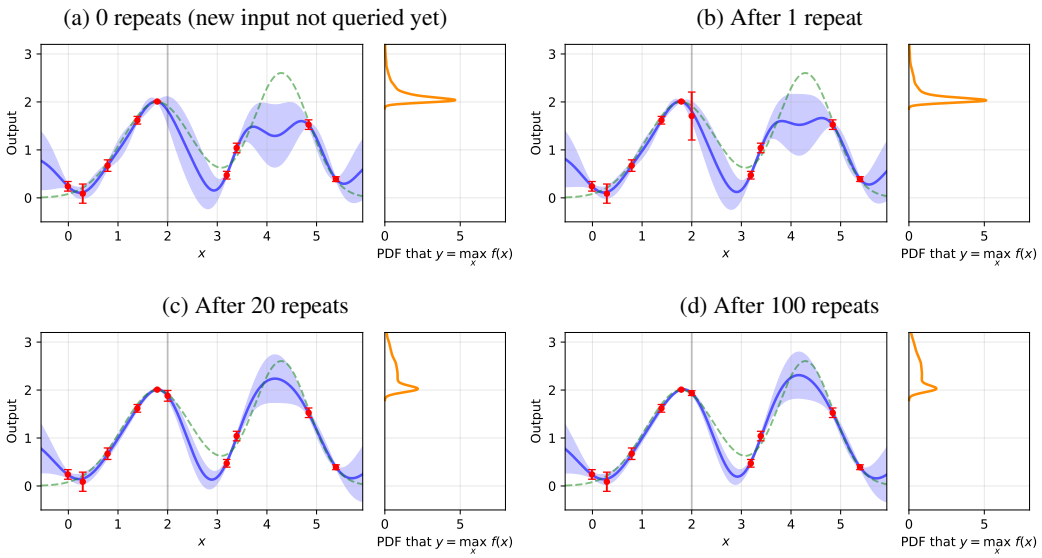

Figure 13: Additional demonstration of why early termination of certain trials does not affect the obtained optimal value. The setup is as done previously in Fig. 12 with queries at $x = 2$. For each subfigure, the left plot represents the modeled GP as shown previously in Fig. 12. In the right diagram, we show the probability density function for the belief of the maximum value $\max_x f(x)$ according to the GP.

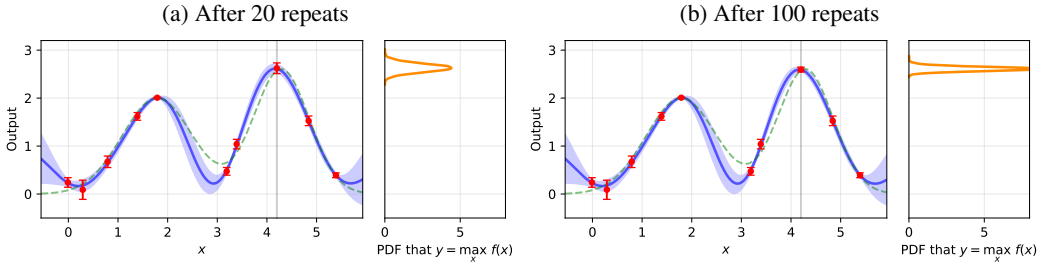

Figure 14: Additional demonstration of why early termination of certain trials does not affect the obtained optimal value. The setup is similar to as done previously in Fig. 12, however instead with queries at $x = 4.2$, and with only 20 repeats and 100 repeats shown (comparable to Figs. 13c and 13d). The information in each subfigure is the same as in Fig. 13.

We will now prove the first half of Thm. 4.1. Given the results in Corollary F.2, we next show that we are able to obtain a GP with good predictive bounds even if some trials are terminated early, i.e., not ran for up to $q_{\max}$ repeats.

Lemma F.3. *Suppose we let*

$$\mu_i(x) = k(x, \mathbf{X}_i)\big(k(\mathbf{X}_i, \mathbf{X}_i) + s^2\mathbf{Q}_i^{-1}\big)^{-1}\mathbf{y}_i\,, \tag{30}$$

$$\sigma_i^2(x) = k(x, x) - k(x, \mathbf{X}_i)\big(k(\mathbf{X}_i, \mathbf{X}_i) + s^2\mathbf{Q}_i^{-1}\big)^{-1}k(\mathbf{X}_i, x) \tag{31}$$

where $\mathbf{X}_i = [x_1 \cdots x_i]$, $\mathbf{y}_i = [\bar{y}_{1,\hat{q}_1} \cdots \bar{y}_{i,\hat{q}_i}]$, *and* $\mathbf{Q}_i = \mathrm{diag}([\hat{q}_1 \cdots \hat{q}_i])$. *If*

$$\beta_i = B + \sqrt{2\log\frac{\det\left(k(\mathbf{X}_i, \mathbf{X}_i) + s^2\mathbf{Q}_i^{-1}\right)^{1/2}}{\delta\det\left(s^2\mathbf{Q}_i^{-1}\right)^{1/2}}} \tag{32}$$

then, with probability greater than $1 - \delta$, *for all* $x \in \mathcal{X}$ *and all* $i = 1, \ldots, N$, *we have*

$$\big|f(x) - \mu_{i-1}(x)\big| \le \beta_i\sigma_{i-1}(x). \tag{33}$$

Algorithm 2 GP-UCB with Repeated Trials

$\mathcal{D}_0 \leftarrow \emptyset$
for $i = 1, \ldots, N$ **do**
  Fit GP on $\mathcal{D}_{i-1}$ to obtain mean μ_{i-1} and variance σ^2_{i-1}
  $x_i \leftarrow \arg\max_{x \in \mathcal{X}} \mu_{i-1}(x) + \beta_i \sigma_{i-1}(x)$
  for $j = 1, \ldots, q_{\max}$ **do**
    Sample $y_{i,j} = f(x_i) + \varepsilon_{i,j}$
  $\bar{y}_{i,q_{\max}} \leftarrow q_{\max}^{-1} \sum_{j=1}^{q_{\max}} y_{i,j}$
  $\mathcal{D}_i \leftarrow \mathcal{D}_i \cup \{(x_i, \bar{y}_{i,q_{\max}})\}$

Algorithm 3 Modified GP-UCB with Early Trial Termination

$\mathcal{D}_0 \leftarrow \emptyset$
for $i = 1, \ldots, N$ **do**
  Fit GP on $\mathcal{D}_{i-1}$ to obtain mean μ_{i-1} and variance σ^2_{i-1}
  $x_i \leftarrow \arg\max_{x \in \mathcal{X}} \mu_{i-1}(x) + \beta_i \sigma_{i-1}(x)$
  for $j = 1, \ldots, q_{\max}$ **do**
    Sample $y_{i,j} = f(x_i) + \varepsilon_{i,j}$
    $\bar{y}_{i,j} \leftarrow j^{-1} \sum_{j'-1}^{j} y_{i,j'}$
    $\mathcal{D}'_{i,j'} \leftarrow \mathcal{D}_i \cup \{(x_i, \bar{y}_{i,j})\}$
    if $j > q_{\min}$ and $\bar{y}_{i,q} < \max_{j<i} \bar{y}_{j,\hat{q}_j} + \tau_q$ **then**
      break // Early termination mechanism
  $\mathcal{D}_i \leftarrow \mathcal{D}'_{i,j'}$

Proof. Given the variance of the mean predictor from Corollary F.2, our scenario can be thought of as having i function measurements with heteroscedastic noise with variances of $s^2/\hat{q}_1, \ldots, s^2/\hat{q}_i$. The variance bounds then follow directly from Lemma 7 in [12] where we substitute $\Sigma_i \to s^2 \mathbf{Q}_i^{-1}$ and $\lambda \to 1$. □

Corollary F.4. *Given Lemma F.3, for all $x' \in \mathcal{X}$, we have $f(x') - \mu_{i-1}(x_i) \leq \beta_i \sigma_{i-1}(x_i)$.*

Proof. We see that

$$\begin{aligned} f(x') - \mu_{i-1}(x_i) &\leq \mu_{i-1}(x') + \beta_i \sigma_{i-1}(x') - \mu_{i-1}(x_i) && \text{by Lemma F.3,} && (34)\\ &\leq \mu_{i-1}(x_i) + \beta_i \sigma_{i-1}(x_i) - \mu_{i-1}(x_i) && \text{by how } x_i \text{ is chosen,} && (35)\\ &= \beta_i \sigma_{i-1}(x_i). && && (36) \end{aligned}$$

□

We now show the cumulative regret of the problem. Let

$$\mathbb{I}[\mathbf{y}_X; \mathbf{f}_X] = \frac{1}{2} \sum_{x'_i \in X} \log\left(1 + \frac{\sigma^2_{i-1}(x'_i)}{s^2/\hat{q}_i}\right), \tag{37}$$

and

$$\gamma_i = \max_{X = [x'_1, \ldots, x'_i] \subset \mathcal{X}} \mathbb{I}[\mathbf{y}_X; \mathbf{f}_X] \tag{38}$$

be the maximum possible information gain across i rounds. We then prove the following result.

Theorem F.5. *Let $x^* = \arg\max_{x \in \mathcal{X}} f(x)$. With probability at least $1 - \delta$,*

$$\sum_{i=1}^{N} f(x^*) - f(x_i) \leq s \beta_N \sqrt{\frac{8 N \gamma_N}{q_{\min}}}. \tag{39}$$

Proof. This result is similar to previous results for UCB-based methods, e.g., Theorem 3 in [33] or Corollary 9 in [12].

With probability at least $1-\delta$, Lemma F.3 holds. We see that

$$\sum_{i=1}^{N}\left(f(x^*)-f(x_i)\right) = \sum_{i=1}^{N}\underbrace{\left(f(x^*)-\mu_{i-1}(x_i)\right)}_{Corollary\ F.4} + \underbrace{\left(\mu_{i-1}(x_i)-f(x_i)\right)}_{Lemma\ F.3} \tag{40}$$

$$\leq \sum_{i=1}^{N} 2\beta_i\sigma_{i-1}(x_i). \tag{41}$$

Since

$$\sum_{i=1}^{N}\sigma_{i-1}^2(x_i) \leq \sum_{i=1}^{N}\frac{s^2}{\hat{q}_i}\frac{\sigma_{i-1}^2(x_i)}{s^2/\hat{q}_i} \tag{42}$$

$$\leq \frac{s^2}{q_{\text{min}}}\sum_{i=1}^{N}\log\left(1+\frac{\sigma_{i-1}^2(x_i)}{s^2/\hat{q}_i}\right) \tag{43}$$

$$\leq \frac{2s^2}{q_{\text{min}}}\gamma_N, \tag{44}$$

we can rewrite (41) as

$$\sum_{i=1}^{N}\left(f(x^*)-f(x_i)\right) \leq \sqrt{\sum_{i=1}^{N}4\beta_i^2}\sqrt{\sum_{i=1}^{N}\sigma_{i-1}^2(x_i)} \qquad \text{by Cauchy-Schwartz,} \tag{45}$$

$$\leq \beta_N\sqrt{4N}\sqrt{\sum_{i=1}^{N}\sigma_{i-1}^2(x_i)} \qquad \text{since } \beta_i \leq \beta_N, \tag{46}$$

$$\leq s\beta_N\sqrt{\frac{8N\gamma_N}{q_{\text{min}}}} \qquad \text{by (44).} \tag{47}$$

□

Remark F.6 (The regret bound in Thm. F.5 is lower when q_{min} increases). We investigate the upper bound in (47) further to see its dependence on q_{min}.

For simplicity, we will let $\mathbf{K} = k(\mathbf{X}_N, \mathbf{X}_N)$. First, we see that

$$\log\det\left(\mathbf{K}+s^2\mathbf{Q}_N^{-1}\right) = \log\det s^2\mathbf{Q}_N^{-1} + \log\det\left(I+s^{-2}\mathbf{Q}_N\mathbf{K}\right) \tag{48}$$

$$\leq \log\det s^2\mathbf{Q}_N^{-1} + \log\det\left(I+s^{-2}q_{\text{max}}\mathbf{K}\right), \tag{49}$$

which means that

$$\beta_N = B + \sqrt{2\log\frac{\det\left(\mathbf{K}+s^2\mathbf{Q}_N^{-1}\right)^{1/2}}{\delta\det\left(s^2\mathbf{Q}_N^{-1}\right)^{1/2}}} \tag{50}$$

$$= B + \sqrt{2\log\frac{1}{\delta} + \log\det\left(\mathbf{K}+s^2\mathbf{Q}_N^{-1}\right) - \log\det s^2\mathbf{Q}_N^{-1}} \tag{51}$$

$$\leq B + \sqrt{2\log\frac{1}{\delta} + \log\det\left(I+s^{-2}q_{\text{max}}\mathbf{K}\right)}. \tag{52}$$

Furthermore, we see that

$$\gamma_N = \max_{X=[x_1',\ldots,x_N']\subset\mathcal{X}}\frac{1}{2}\sum_{x_i'\in X}\log\left(1+\frac{\sigma_{i-1}^2(x_i')}{s^2/\hat{q}_i}\right) \tag{53}$$

$$\leq \max_{X=[x_1',\ldots,x_N']\subset\mathcal{X}}\frac{1}{2}\sum_{x_i'\in X}\log\left(1+\frac{\sigma_{i-1}^2(x_i')}{s^2/q_{\text{max}}}\right). \tag{54}$$

Therefore we see that both β_N and γ_N are upper bounded by terms which are independent of q_{min}, and so the constants in the upper bound provided in Thm. F.5 do not hide any additional dependencies with respect to q_{min}. This shows that the upper bound of cumulative regret from (47) decays at a rate of $1/\sqrt{q_{\text{min}}}$.

We will now prove the second half of Thm. 4.1. We first prove the following result.

Lemma F.7. *Define* $c_1 \triangleq \sqrt{2\log(2Nq_{\max}/\delta)}$. *With probability at least* $1-\delta$, *for all* $i = 1, \ldots, N$ *and all* $q = 1, \ldots, q_{\max}$, *we have*

$$\left|\bar{y}_{i,q} - f(x_i)\right| \leq \frac{c_1 s}{\sqrt{q}}. \tag{55}$$

Proof. From Corollary F.2, we know that the $\bar{y}_{i,q}$ is normally distributed with mean $f(x_i)$ and standard deviation $s/\sqrt{q}$. By Chernoff bounds, for each $i = 1, \ldots, N$ and each $q = 1, \ldots, q_{\max}$, we would have $\bar{y}_{i,q} - f(x_i) > c_1 s/\sqrt{q}$, and $f(x_i) - y_{i,q} > c_1 s/\sqrt{q}$ where either event happens with probability no greater than $\delta N/2q_{\max}$. This means that with probability no greater than $\delta/Nq_{\max}$, we have $|y_{i,q} - f(x_i)| > c_1 s/\sqrt{q}$. Therefore, by union bound, we have for all $i = 1, \ldots, N$ and each $q = 1, \ldots, q_{\max}$, we would have $|\bar{y}_{i,q} - f(x_i)| \leq c_1 s/\sqrt{q}$ with probability greater than $1 - (\delta/Nq_{\max})(Nq_{\max}) = 1 - \delta$. □

Theorem F.8. *Define*

$$\tau_q = c_1 s \left(\frac{1}{\sqrt{q_{\min}}} + \frac{1}{\sqrt{q}}\right). \tag{56}$$

Then, with probability at least $1-\delta$, *for all* $i \leq N$, *if we have* $f(x_i) < \max_{j<i} f(x_j)$, *then* $\hat{q}_i < q_{\max}$.

Proof. With probability at least $1 - \delta$, Lemma F.7 applies.

To prove the statement above, we show its contrapositive. Suppose we have $\hat{q}_i = q_{\max}$, or that the trial for x_i does not terminate early. This implies that $\bar{y}_{i,q} \geq \max_{j<i} \bar{y}_{j,\hat{q}_j} + \tau_q$ for all $q = q_{\min}, \ldots, q_{\max}$. For any q in this range, we would then have

$$\begin{aligned}
f(x_i) &\geq \bar{y}_{i,q} - \frac{c_1 s}{\sqrt{q}} && (57)\\
&\geq \max_{j<i} \bar{y}_{j,\hat{q}_j} + \tau_q - \frac{c_1 s}{\sqrt{q}} && (58)\\
&\geq \max_{j<i} f(x_j) - \frac{c_1 s}{\sqrt{q_{\min}}} + \tau_q - \frac{c_1 s}{\sqrt{q}} && (59)\\
&= \max_{j<i} f(x_j). && (60)
\end{aligned}$$

This proves the contrapositive which in turn proves the original statement. □

Finally, Thms. F.5 and F.8 can be combined with appropriate union bounds to achieve a more formal version of Thm. 4.1.

F.3.3 Ablation Studies on Toy Examples

In Fig. 15, we provide a brief empirical demonstration of efficiency gains due to early termination. We see that when the noise variance is too high, querying the function once per input would give measurements which are too noisy to give good information. Meanwhile, by repeating each query a maximum number of times, we can obtain a good estimate of the actual function and allow the BO algorithm to arrive at the optimal using few queries. However, we see that when early termination is allowed, we can still arrive at the optimal input as before, while not requiring all queries to be repeated the maximum number of times. This shows that early termination allows for efficiency gains while minimally sacrificing on the actual optimization process.

In practice, since it is difficult to determine γ_N, β_N, s, and c_1 exactly, we instead fix β_i and τ_q to some constant. In OPPA, we choose $\beta_i = 1$ and $\tau_q = 10^{-3}$. We find that these values work well for our methods. Furthermore, in our proofs we do not consider the constrained BO setting. Despite this, the early termination can still be used in practice to achieve good results which we show in the experiments.

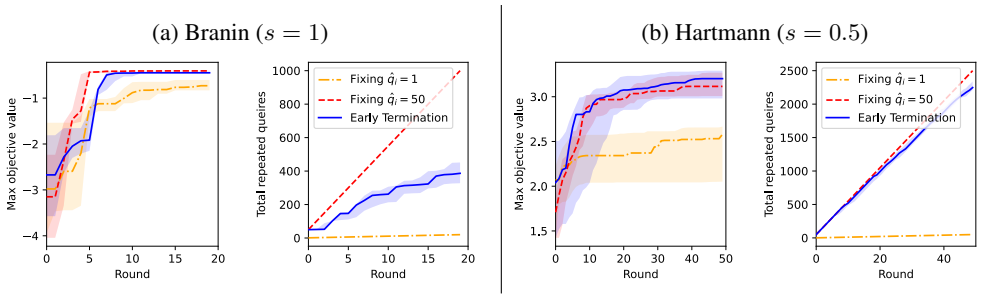

Figure 15: Results of BO with early termination (with $q_{\min} = 1$) on different synthetic functions where each query has different noise levels. For each case, we show the best queried objective value (left plot), and the cumulative number of total repeated queries made with each BO iteration (right plot).

G Pseudocode of OPPA

We present the pseudocode for OPPA in Algorithm 4.

In practice, we find that fixed hyperparameter values (i.e., setting $\beta_t = 1$, $\tau_q = 10^{-3}$, and $q_{\min} = 5$ in all iterations as done in our main experiments) gives consistent results since the parameters are generally robust to different choices of hyperparameter values anyway.

In the experiments, the value of $q_{\max}$ are set in accordance to Table 2 depending on the benchmark; however in practice can be set as large as the practitioner wants depending on how accurately they would like to measure the actual throughput of the PC. As plotted in Fig. 16, we find that after a certain point, a larger number of repeats will typically not have large effects on the measured throughput of a PC, showing that OPPA is quite robust to different choices of $q_{\max}$. For OPPA, larger $q_{\max}$ is more tolerable since the early termination mechanism will not exhaust such budget anyway.

We also consider removing outliers which are beyond two times the IQR from the mean; this is be more lenient towards fluctuating training effects, however can also be set to 1.5 times the IQR as typically done as well with little consequences, as described in App. F.2.

Algorithm 4 OPTIMIZER FOR PARALLELISM CONFIGURATIONS (OPPA)

Generate all valid PCs $\mathcal{H}$
$i \leftarrow 1$
while time budget not exhausted **do**
  if $i < N_{\text{random}}$ **then**
    Select H_i randomly
  else
    // Step ① – Modeling throughput and memory usage
    Construct $\mu_{\mathcal{R},i-1}$ and $\sigma^2_{\mathcal{R},i-1}$ according to (23) and (24) respectively
    Construct $\mu_{\mathcal{M},i-1}$ and $\sigma^2_{\mathcal{M},i-1}$ according to (25) and (26) respectively
    // Step ② – Selecting the next PC to trial
    $H_i \leftarrow \underset{H \in \mathcal{H} \setminus \{H_1,\ldots,H_{i-1}\}}{\arg\max}$ $\text{cUCB}_i(H)$ where cUCB_{i-1} is defined in (27)
  // Step ③ – Trialing selected PC
  for $q = 1, \ldots, q_{\max}$ **do**
    Measure training step time as $t_{i,j}$
    Compute $\bar{r}_{i,q}$ and $\sigma^2_{\bar{r}_{i,q}}$ according to (28)
    if $I_{i,q} = 0$ **then**
      break // Early termination condition from (3)
  Measure maximum memory usage as m_i
  $\hat{q}_i \leftarrow q$ to track the number of training steps ran in round i
  $i \leftarrow i + 1$
return H_{i^*} where $i^* = \arg\max_{i\,:\,(m_i < M_0) \wedge (\hat{q}_i = q_{\max})} \bar{r}_{i,\hat{q}_i}$

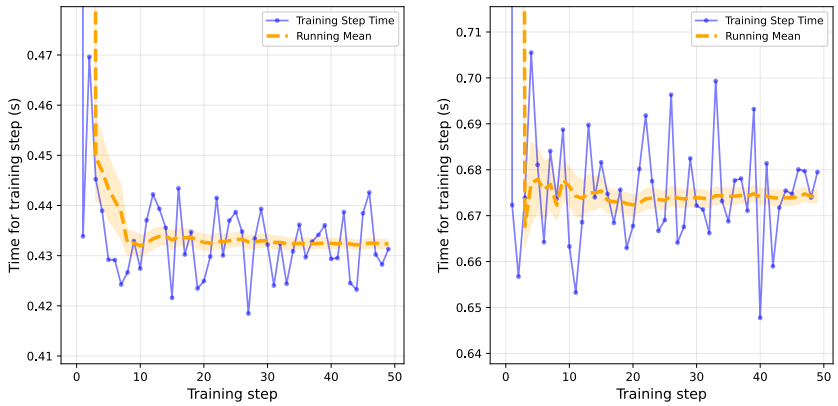

Figure 16: The effect of number of training steps repeatedly measured on the predicted throughput. The blue lines represent a training trial and the measured time per training step. The orange line represents the average training time (i.e., reciprocal of throughput) predicted up to that certain training step.

H Additional Information on Experimental Setup

H.1 Training and Hardware Configurations

We list the models used in our experiments in Table 2, along with the allotted search time and how many trials we repeat on them. All models used are based on the transformer architecture, and were retrieved from Huggingface.

Note that in all of our plots, we plot the median value (with a line) and also the lower and upper quartiles (with a fainter band over and under the line). We do so since we find that the values are often asymmetrically skewed, and therefore opted to show the quartile values to more accurately represent the distribution of these values. Also note that the repeated trials were reduced for larger models due to restrictions in compute budget.

Table 2: Details of models used in our experiments and the corresponding training scenario

Case	Model	# Params	Batch size	Max. seq. length	Search Time	$q_{\max}$	Repeats
`BERT`	BERT Base Uncased	110M	256	256	20 mins	50	10
`Qwen2-1.5b`	Qwen-2	1.5B	64	1024	20 mins	30	10
`Llama3-1b`	Llama 3	1B	64	1024	60 mins	20	5
`Llama2-7b`	Llama 2	7B	256	1024	60 mins	30	5
`Qwen3-32b`	Qwen-3	32B	256	8192	80 mins	30	5

In Table 3, we list the hardware configuration used in our experiments. The hardware configurations used are based on the resources that are available to the authors.

Table 3: Configurations of tested hardwares.

Config. Name	GPU Model (Memory)	GPUs per Node	# Node	Multi-Node Characteristic
8 GPUs	NVIDIA RTX A5000 (24GB)	8	1	-
16 GPUs	NVIDIA RTX 3080 (10GB)	8	2	Docker Overlay Network
32 GPUs	NVIDIA A100 (40GB)	4	8	High-Performance Compute
128 GPUs	NVIDIA GH200 (96GB)	4	32	High-Performance Compute

H.2 Other Methods Ran For Comparison

We list the other methods we have ran along with their implementation details here.

- RANDOM. This involves randomly selecting a PC from $\mathcal{H}$ to trial in each round until the time budget is exhausted.

- XGBOOST [3]. This is the method DEEPSPEED [28] uses to configure the PC, and is adapted to work with the hyperparameters in our PC. The method involves training an XGBOOST model based on the measured throughput, then selecting the next PC to trial as the one whose predicted throughput is the highest. This is repeated until time budget is exhausted.
- COST-MODEL. This involves using the cost model as described in Apps. D.1 and D.2, learned based on several randomly selected PCs, to obtain a prediction of throughput and maximum memory usage, and perform a one-shot selection of the best PC according to the predictions.
- VANILLA-BO. This performs BO whose GP has a constant mean and a Matern kernel with $\nu = 5/2$. The cUCB criterion is used for PC selection. The BO loop is implemented using BOTORCH [1].
- OPPA. This is the method proposed in Sec. 4 which involves modifying BO to include parallelism-informed GP prior beliefs and early trial termination. The hyperparameters used are as stated in App. G.

We note that due to the search space employed for $\mathcal{H}$, we do not consider methods which performs non-adaptive optimization with a cost model. This is because those methods optimize with respect to the computation graph rather than the hyperparameters which we discussed in App. C.1, and since they do not use the same information as OPPA to perform optimization, making it futile to compare between the two since they focus on optimizing different aspects of training parallelism. Nonetheless, we provide some comparisons with selected methods of such nature, namely, [15] and [19] in Fig. 9.

I Additional Results

I.1 Plots of Best Achieved Throughput vs. Other Quantities

In Fig. 17, we plot the best achieved throughput vs. the number of training trials that have been ran. We see that in this view, OPPA still outperforms other methods. While the margin may be smaller in some instances, we see that OPPA is able to achieve the good results more consistently as seen by the error bars when compared to some of the other methods. This also demonstrates that the prior belief used in OPPA alone would have helped in achieving a better performance regardless of the early termination mechanism in OPPA.

In Fig. 18, we show the achieved throughput is plotted against the number of training steps run in the training trials, showing that the difference in efficiency of OPPA becomes more pronounced. From these results see that OPPA is both more time-efficient and query-efficient which can be useful when the overhead to run one trial may become higher, for example when the framework is adapted to run on a cluster with a job scheduler.

I.2 Optimal PCs recovered by OPPA

In Tables 4 and 5, we show the PCs that were recovered by OPPA for training scenarios ran on the COLOSSAL-AI and NEMO frameworks respectively. Note that the optimal PCs chosen match quite well with intuition where for smaller models DP tends to be prioritized. Meanwhile for larger models and training scenarios which are done across multiple nodes, PP and potentially TP is prioritized. In all of these cases, there is a range for the hyperparameters within the potential PC, which suggests that multiple choices of PC can achieve similar throughput.

I.3 Flexibility Across Different Parallel Training Frameworks

Another advantage of adaptively selecting actual training trials to run can be seen when we change the parallel training framework used to train the NN. In Fig. 19, we run similar experiments as in Fig. 4, however instead performing training on NEMO [13]. In these experiments, we consider additional hyperparameters within our PC, such as the size of the sequence parallelism dimension. We see that compared to Fig. 4, the obtained maxima are different because the training processes are implemented differently across the two frameworks, and the fact that the adjustable hyperparameters in the PC are also different. Regardless, we see that even though most methods can eventually recover the optimal

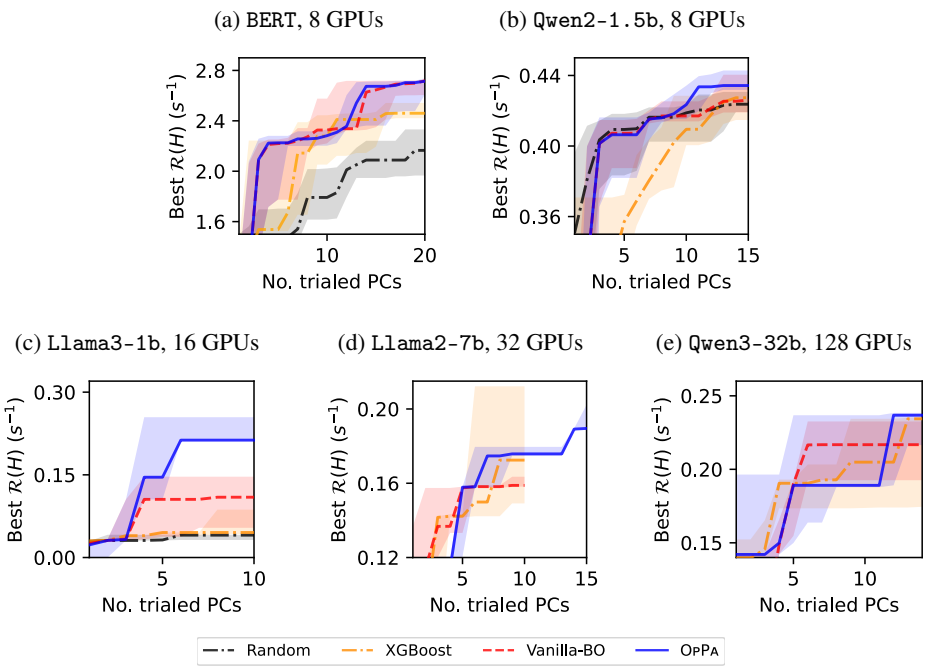

Figure 17: Results of the best obtained throughput (higher is better) plotted against the number of PCs that have been trialed. The lines represent the median value of the best obtained throughput across five trials, while the error bar represent the quartile values. Note that for the experiments on 32 GPUs, we are unable to run the optimization beyond the allotted time due to resource constraints and therefore are only able to plot some methods for a fewer number of queried PCs.

Table 4: Example of optimal PCs selected by OPPA in different training scenarios when training on COLOSSAL-AI framework. Values are based on the found optimal PCs across multiple repeated trials. A range of value shows that a certain parameter shows a spread across multiple trials (i.e., no strong preference towards one value), while a dash shows that the parallelism dimension associated with that hyperparameter is not used. Note that these may not be the best PCs for the training scenarios, but are instead only examples of what are recovered by OPPA.

Hyperparameter	BERT, 8 GPUs (Fig. 4a)	Qwen2-1.5b, 8 GPUs (Fig. 4b)	ViT, 8 GPUs (Fig. 21)	Llama3-1b, 16 GPUs (Fig. 8a)	Llama2-7b, 32 GPUs (Fig. 8b)
DP size (dp)	8	4	8	1	2
TP size (tp)	1	1	1	1	1
PP size (pp)	1	2	1	16	16
DP bucket size	1 – 64	1 – 4096	1 – 64	-	1 – 4096
ZeRO stage	0	1	0	-	1
ZeRO bucket size	-	1 – 64	-	-	64 – 4096
Overlap ZeRO communication	-	True/False	-	-	False
Overlap DP AllGather	-	True/False	-	-	False
# microbatches (mb)	-	8	-	64	32
# model chunks (mc)	-	1 – 2	-	1	1
Overlap P2P for PP	-	True/False	-	False	True/False
Grad. checkpointing	False	False	True	False	False

PC, OPPA is able to do so much more rapidly and, more importantly, much more consistently. The latter fact can be seen in the error bars of the other methods which are much larger than that of OPPA. This demonstrates that OPPA does not overfit to any one specific training framework, but instead can simultaneously cater to different training frameworks.

I.4 PC Optimization for Other Models

In Fig. 21, we presented the results for tuning the PC for ViT model [6]. We see that the results here show that OPPA is able to select better PCs compared to the other methods, consistent with other results in the paper.

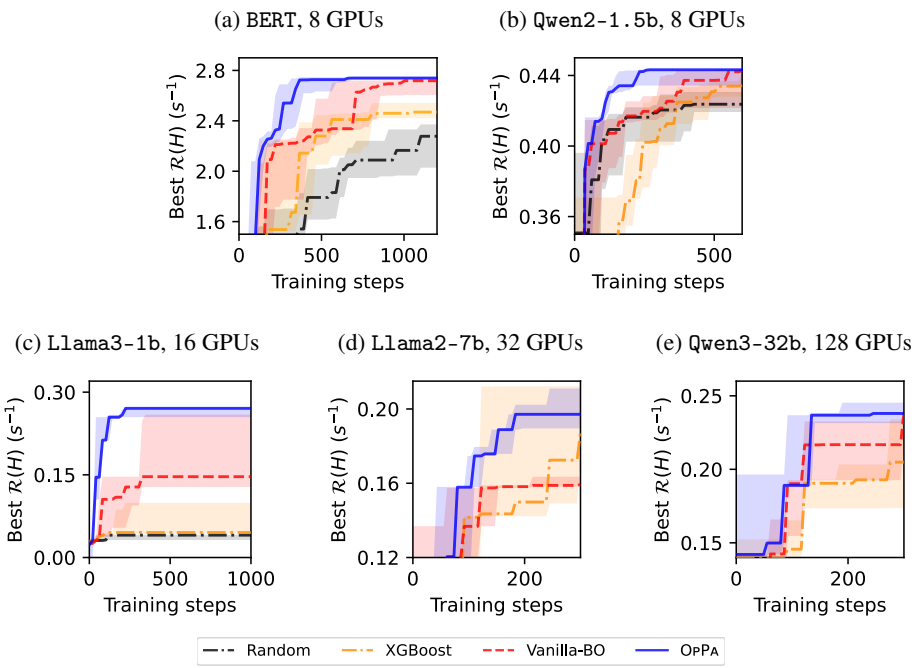

Figure 18: Results of the best obtained throughput (higher is better) plotted against the total number of training steps ran during in the training trials. The lines represent the median value of the best obtained throughput across five trials, while the error bar represent the quartile values.

Table 5: Example of optimal PCs selected by OPPA in different training scenarios when training on NEMO framework. The interpretation is as in Table 4.

Hyperparameter	BERT, 8 GPUs (Fig. 19a)	Qwen2-1.5b, 8 GPUs (Fig. 19b)	MoE, 8 GPUs (Fig. 22)	Qwen3-32b, 128 GPUs (Fig. 8c)
DP size (dp)	8	4	8	16–32
TP size (tp)	1	1	1	4
PP size (pp)	1	2	1	1 – 2
SP size	1	1	1	1 – 4
EP size	-	-	2	-
CP size	-	-	-	1
DP bucket size	1 – 64	1 – 4096	1 – 4096	1 – 4096
ZeRO stage	0	0	0	0
Overlap ZeRO communication	-	-	-	-
Overlap DP AllGather	False	False	True	True
# model chunks (mc)	-	1	-	-/4
Overlap P2P for PP	-	-/True/False	-	True/False
Grad. checkpointing	False	False	False	False

Additionally, in Fig. 22, we presented the results for tuning the PC for transformer-based Mixture-of-Experts (MoE) model [30] with the additional tuning of the expert parallelism (EP) degree being performed by the same framework in addition to the existing DP, TP and PP. For the experiments we consider parallel training of a model with 16 transformer units, 32 attention heads and 32 experts. Each trial is ran for up to $q_{\max} = 50$ steps, and in OPPA, we set $q_{\min} = 10$ to account for higher variation in training step times. In the results, we again see consistently better performances compared to the other competing methods. Specifically, even if OPPA may eventually lead to similar results to vanilla BO at the end of the optimization process, OPPA is able to do so more consistently (lower variance across random runs), and is able to arrive at the optimal PC much more rapidly and efficiently. These results further demonstrate that OPPA is able to also generalize to other models as well.

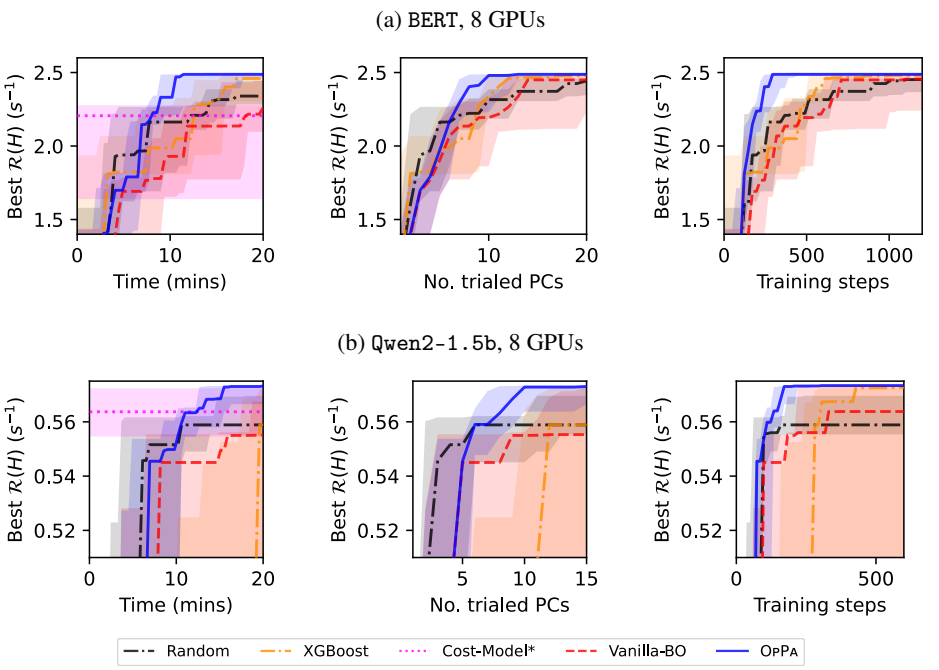

Figure 19: The best obtained throughput (higher is better) vs. the duration each method has been run for, when training on a system with a single node and using the NEMO framework [13]. Both cases train NN with identical architectures as the experiments in Figs. 4a and 4b respectively, and are ran on a single node.

I.5 Predicted Throughput and Memory by Parallelism-Informed GP Prior Beliefs

In Figs. 23 to 25, we compare the modeled throughput with the actual values in different training scenarios. We see that in this case, the parallelism-informed GP prior beliefs allow for the values to be modeled adequately well, but more importantly, allow for the PC which achieves the best throughput to also have the highest values, and therefore be identified correctly. We find that for BO, surrogate models only need to model the good PCs well in order to select a good PC in the end. Meanwhile, when not using the parallelism-informed prior beliefs, the GP posterior beliefs learn the patterns much less efficiently or do not learn them at all. This correlates well with the results in the main text where standard BO selects a worse PC compared to OPPA which uses a better GP prior belief.

In Fig. 26, we compare the modeled maximum memory with the actual measured value. In both cases, a GP has been used, however, with and without a parallelism-informed GP prior belief since only VANILLA-BO and OPPA are the only methods we tested which explicitly models the memory usage. Here, we see that OPPA is able to better model the memory usage due to its use of the GP prior belief. This is reflected in the confusion matrices which shows that after training, OPPA is able to more accurately detect when a certain PC will result in out-of-memory errors.

To additionally demonstrate the interpretability of the GP for the surrogate model, in Table 6, we show the results for the lengthscales learned by the kernel (as given in (20)). We see that hyperparameters that have larger effects on the resulting throughput or are less well-modeled by our GP prior belief will typically correspond to the shorter lengthscales. For example, for the training of BERT, we see that the parameters for TP dimension size and for the number of microbatches (for PP) have shorter lengthscales. This matches our intuition where the throughput would be more sensitive to the increased TP or PP being used (for the worse).

I.6 Effects of Prior Misspecification

To investigate the robustness of our method with respect to a misspecified prior, we perform experiments to see how OPPA behaves as our cost-model prior becomes increasingly inaccurate. To do so, we add a perturbation term into our cost function where we increase the magnitude of the perturbation

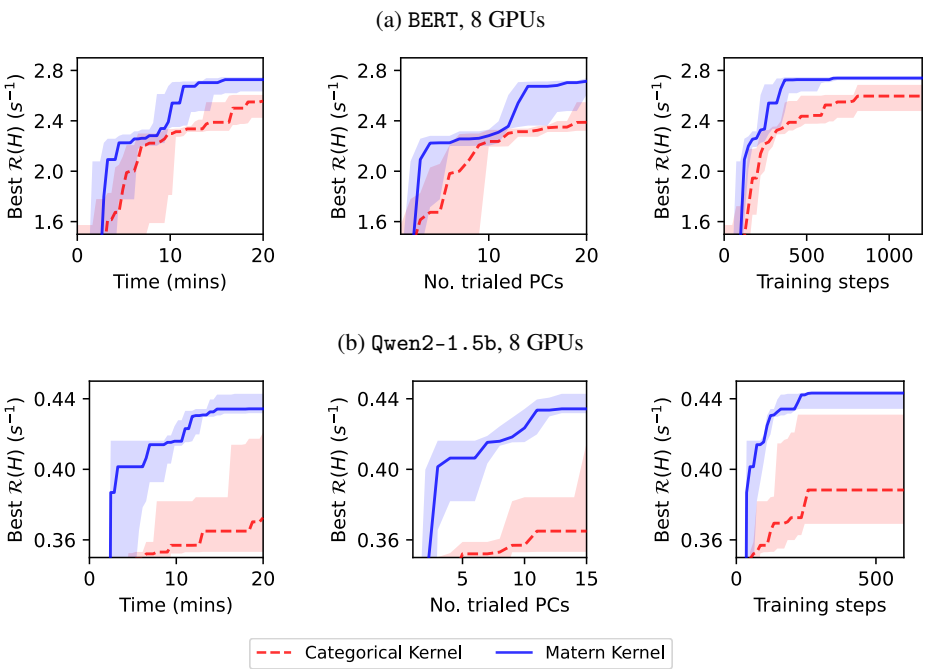

Figure 20: The best obtained throughput (higher is better) vs. the duration OPPA has been run for, when changing from the Matern kernel to the categorical kernel [4]. Both cases train NN with identical architectures as the experiments in Figs. 4a and 4b respectively (with the results for the Matern kernel being exactly the same as in those figures), and are ran on a single node.

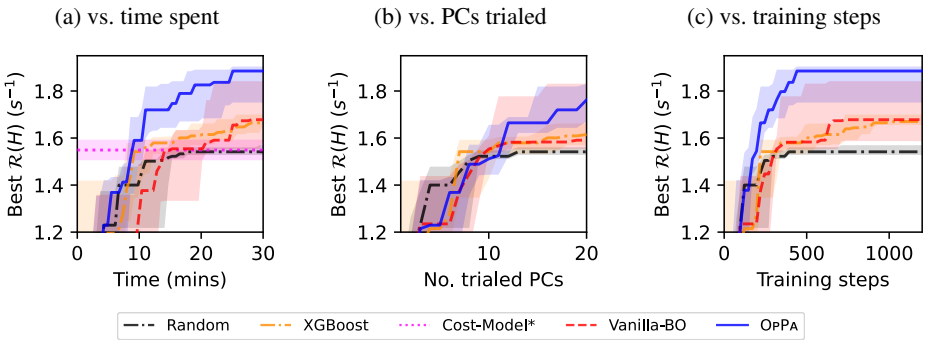

Figure 21: Results for training ViT model [6] with batch size of 256.

term up to about 25% and 50% that of the maximum throughput obtained. We present the median obtained throughput across 5 random trials in Table 7. We see that even when the cost-function prior is adversarially constructed (by knowingly adding an incorrect term into the cost function), we are still able to obtain good performances to the unperturbed cost-model prior even if the convergence is slightly slower. This suggests that even in this extreme case, the GP is able to correct for the inaccuracies in the cost-prior effectively.

In practice, prior misspecification typically will due to the cost function not being sufficiently complex to match the actual parallel training dynamics, because of incomplete or inaccurate domain knowledge about the actual system rather than due to an adversarial construction of the cost function. This is the case in the cost function we have chosen in our paper where there is a discrepancy between the cost function alone and the actual throughput as demonstrated in Fig. 6c, resulting from our cost function not modeling the effects of all hyperparameters in the PC. Under practical scenarios, we therefore would not expect the results to be as extreme as what we have seen in the presented results, and that a GP should be able to effectively model the throughputs.

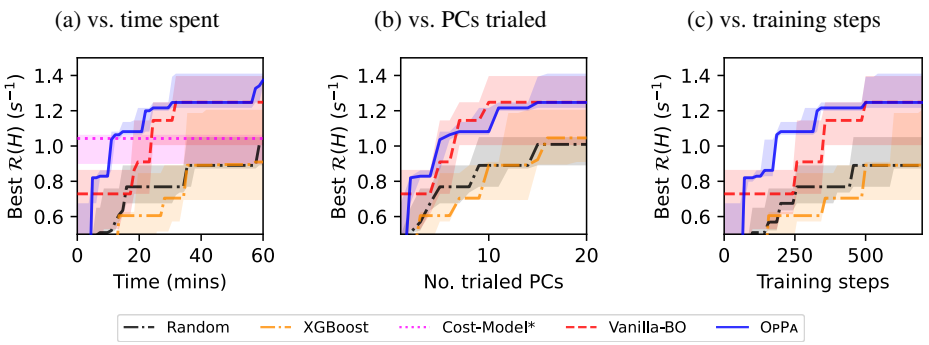

Figure 22: Results for training Mixture-of-Experts [30] models.

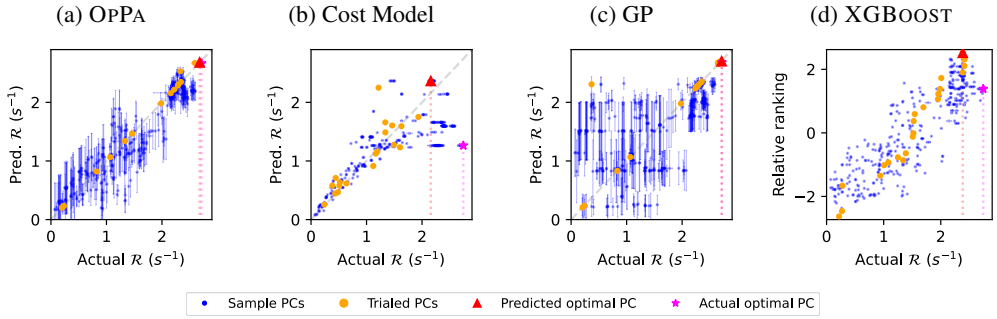

Figure 23: Comparison of modeled throughput vs. the actual throughput for training of `BERT` model on 8 GPUs after 20 training trials.

I.7 Additional Results for Ablation Studies of Components in OPPA

In Fig. 27, we demonstrate how early termination and parallelism-informed GP prior beliefs affect the overall achieved throughput. First, we see that when parallelism-informed GP prior beliefs are used, the performance is no worse than when no GP prior belief is used, although this benefit is more pronounced for the `Qwen2-1.5b` example, possibly due to the increased complexity in the training setup. Meanwhile, with early termination, we see that the performance is better in terms of time and number of training steps needed, while not sacrificing the performances when considering the number of PCs that are trialed to achieve a certain performance. This shows that the benefit gain comes from being able to shorten the duration of the training trials while not sacrificing the throughput predictions.

I.8 Effect of $q_{\min}$ on OPPA performance

In Fig. 28, we see how the choice of $q_{\min}$ affects the achieved throughput. For the `BERT` case, we see that early termination clearly improves the time required for optimization, as seen where when $q_{\min} = q_{\max}$ the obtained PC is the worst when all methods are allotted the same amount of time. As $q_{\min}$ decreases, we see that there is less drop in the amount of time required since each training step is dominated by the time to setup each training trial. However, we still see that when we plot the number of training steps for the optimization, we see that a smaller $q_{\min}$ will require fewer training steps to arrive at the same optimal PC. However, this trend breaks down when $q_{\min}$ is too small, likely since the value obtained is too noisy to give good information. Nonetheless, even in this case, we stil obtain good results. For the `Qwen2-1.5b` case, similar trends can be seen where reducing $q_{\min}$ is able to reduce the time and the number of training steps required to find the optimal PC up to a certain point.

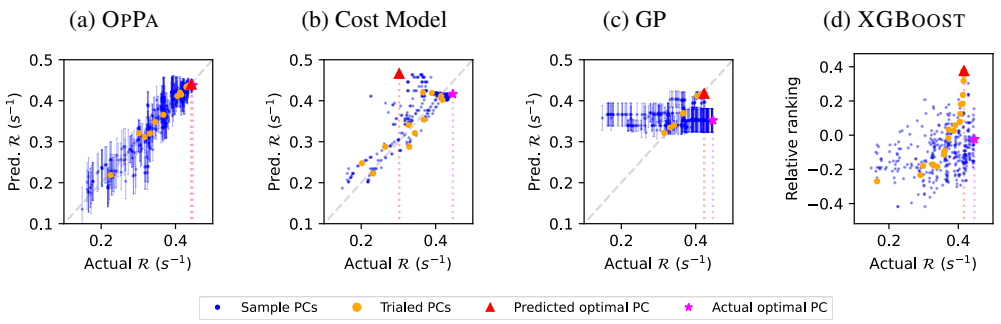

Figure 24: Comparison of modeled throughput vs. the actual throughput for training of `Qwen2-1.5b` model on 8 GPUs after 20 training trials.

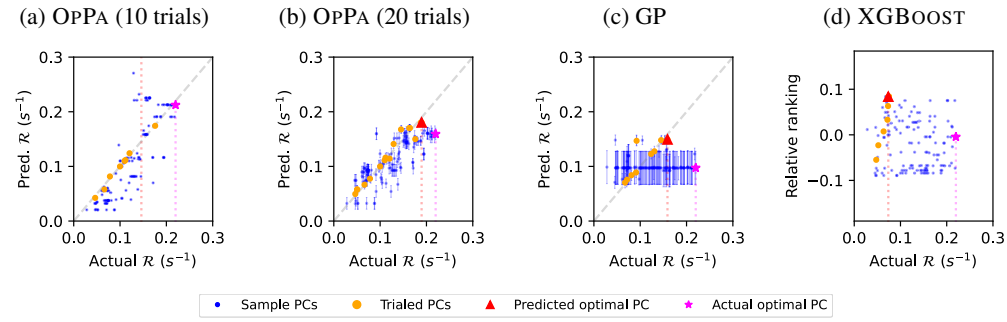

Figure 25: Comparison of modeled throughput vs. the actual throughput for training of `Llama-2` model on 32 GPUs for, in order, OPPA after 10 trials, OPPA after 20 trials, GP after 10 trials and XGBOOST after 10 trials. Note that among the three methods, only OPPA ran for up to 20 trials given the time constraint.

J Limitations and Broader Impacts

While there are many other factors of parallel training that we could optimize, we have mainly considered hyperparameters commonly found in existing parallel NN training frameworks which would generally be tuned manually by practitioners. We believe that OPPA can also be extended to optimize in other more sophisticated PC search spaces that may arise in practice as well. Maximizing the throughput during NN training would allow the same amount of computation to possibly be done in a more efficient manner, both in terms of time and compute resources. While this may allow faster development of NNs for both good and bad use cases, overall it would still have a positive impact since it allows for higher efficiency which reduces waste in computation time and other feasible resources that come with it.

(a) OPPA

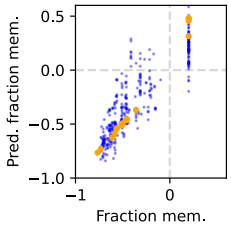

	Predicted Feasible	Predicted OOM
Actual Feasible	296	16
Actual OOM	4	84

(b) BO

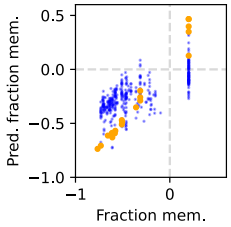

	Predicted Feasible	Predicted OOM
Actual Feasible	309	3
Actual OOM	54	34

(c) Cost Model

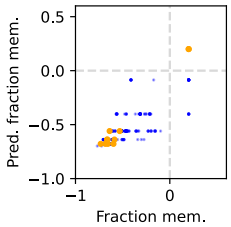

	Predicted Feasible	Predicted OOM
Actual Feasible	312	0
Actual OOM	23	65

Figure 26: Comparison of modeled maximum memory usage vs. the actual maximum memory usage for training of `Qwen2-1.5b` model on 8 GPUs after 20 training trials. In each row, the left hand graph shows the predicted value vs. the actual value (with the predictive variance are omitted for clarity), while the right hand table is the confusion matrix.

Table 6: Example of the log lengthscales learned by the kernel of the GP for the throughput. The bolded value are to highlight hyperparameters with particularly shorter lengthscales.

Hyperparameter	`BERT`, 8 GPUs	`Qwen2-1.5b`, 8 GPUs
DP size (`dp`)	1.877	5.233
TP size (`tp`)	**-1.071**	6.024
PP size (`pp`)	2.293	**-1.849**
DP bucket size	3.484	5.994
ZeRO stage	0.434	5.279
ZeRO bucket size	3.402	6.516
Overlap ZeRO communication	3.949	7.581
Overlap DP AllGather	3.822	7.589
# microbatches (`mb`)	**-1.322**	**-1.741**
# model chunks (`mc`)	-0.293	0.124
Overlap P2P for PP	3.854	6.974
Grad. checkpointing	-0.334	6.586

Table 7: Effect of perturbing the GP prior belief on the resulting optimization process. The values reported are the median throughput obtained for the PC found after certain number of minutes of running OPPA with the perturbed prior belief.

Percent perturbation magnitude	10 mins. of search	20 mins. of search
0 (original prior)	0.425	0.446
About 25	0.424	0.447
About 50	0.415	0.447

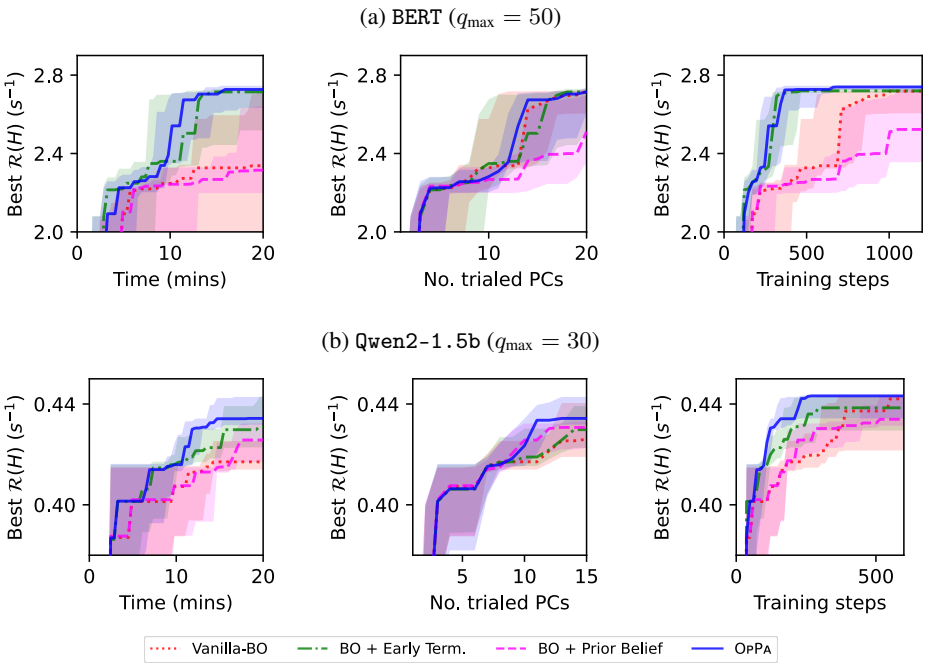

Figure 27: The effects of different components of OPPA on the optimal PC found. In each row, we present the results in a certain training setup as noted in the subheader. We present the obtained throughput versus, from left to right, the time the method has been ran for, the number of unique PCs trialed, and the number of training steps that has been ran across all of the trials.

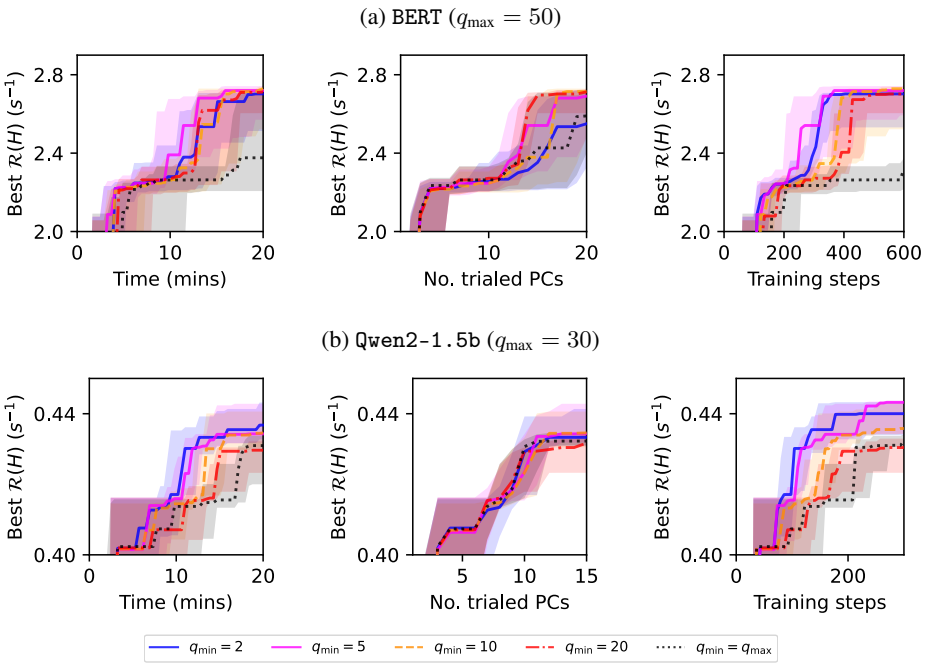

Figure 28: The effects of $q_{\min}$ on the optimal PC found. In each row, we present the results in a certain training setup, where we present the obtained throughput versus, from left to right, the time the method has been ran for, the number of unique PCs trialed, and the number of training steps that has been ran across all of the trials.